



**Politecnico  
di Torino**

**Politecnico di Torino**

Corso di Laurea Magistrale in Ingegneria Meccanica-Progettazione Meccanica

A.a. 2021/2022

Sessione di Laurea Marzo-Aprile 2022

# **Friction Stir Welding of Titanium**

Analysis of optimal process parameters and joint characterization

Relatore:

*Lombardi Franco*

Co-Relatori:

*De Maddis Manuela*

*Russo Spina Pasquale*

Candidato:

*Bertolini Carmine*

## ACKNOWLEDGMENTS

*I feel obliged to dedicate this page of the present paper to the people who have supported me in the writing of it.*

*First of all, I would like to thank my supervisor, Professor Franco Lombardi, and my co-rapporteurs, Professor Manuela De Maddis and Professor Russo Spina Pasquale, who were always ready to give me the right indications in every phase of the elaboration. Thanks to you I have increased my knowledge and skills.*

*A special thanks goes to my Tutor Engineer Lunetto Vincenzo, who helped me to conduct research, the subject of the paper, at J-Tech. Thank you for being always available and for giving me so many fundamental advices.*

*I would like to thank my family, because without them I would have never been able to undertake this course of study and for always supporting me in times of difficulty.*

*I would like to thank my closest friends, who have been close to me over the years and with whom I have shared both joy and suffering.*

*A mia madre Anella e mio padre Nicola.*

# CONTENTS

<b>1. INTRODUCTION FRICTION STIR WELDING .....</b>	<b>4</b>
<b>1.1. ADVANTAGES AND DISADVANTAGES OF FSW .....</b>	<b>5</b>
<b>1.2. DESCRIPTION OF THE PROCESS AND JOINT AREA .....</b>	<b>6</b>
<b>1.3. DEFECTS .....</b>	<b>7</b>
<b>1.4. TYPES OF JOINT CONFIGURATION .....</b>	<b>8</b>
<b>1.5. DESIGN OF TOOL FOR FSW .....</b>	<b>10</b>
<b>1.6. TITANIUM AND TITANIUM ALLOYS.....</b>	<b>12</b>
<b>2. FSW OF TITANIUM .....</b>	<b>16</b>
<b>2.1. DEFECTS IN TITANIUM JOINTS .....</b>	<b>16</b>
<b>2.2. FSW OF COMMERCIALY PURE TITANIUM IN LAP AND BUTT JOINT CONFIGURATION.....</b>	<b>19</b>
<b>2.3. DESIGN OF TOOL FOR FSW OF TITANIUM .....</b>	<b>30</b>
<b>2.4. APPLICATIONS FIELDS OF FSW OF TITANIUM .....</b>	<b>38</b>
<b>3. EXPERIMENTAL PROCEDURE.....</b>	<b>44</b>
<b>4. RESULTS AND DISCUSSIONS.....</b>	<b>45</b>
<b>4.1. WELDING OF 1 MM Ti SHEETS .....</b>	<b>45</b>
<b>4.2. WELDING OF 2 MM Ti SHEETS .....</b>	<b>49</b>
<b>5. CONCLUSIONS.....</b>	<b>53</b>
<b>ACKNOWLEDGMENTS .....</b>	<b>2</b>
<b>REFERENCES.....</b>	<b>54</b>

# 1. INTRODUCTION FRICTION STIR WELDING

Friction stir welding (FSW) was invented at The Welding Institute (TWI) of the United Kingdom in 1991. It is an innovative welding process that permit to obtain a joint between two sheets of metallic material using a solid-state joining technique. FSW is considered a great discovery that has allowed a better development in metal joining especially for aerospace application. It has gained a particular interest due to the avoidance of solidification problems that in other welding process are present. Initially applied to low melting metals such as aluminium alloys and magnesium alloys, recently the FSW is applied also high melting metals such as steel and especially the titanium alloys[1]. It is a “green” technology thanks its energy efficiency and environment friendliness compared to the other welding method. Another advantage is the possibility to join different kind of metals without to take in consideration the compatibility of composition because the metal is not melted and therefore materials with different melting points can be processed[2]. It has been demonstrated that FSW produces joint strong and ductile in system which sometimes have proved difficult using conventional welding techniques. The process is most appropriate for components which are long and flat (sheet and plates) but may be adapted also for pipe and other configuration[3].

## 1.1. ADVANTAGES AND DISADVANTAGES OF FSW

### **Metallurgical and Technological benefit:**

- ✓ Solid-phase process.
- ✓ Low distortions.
- ✓ Good dimensional stability and repeatability.
- ✓ No loss of alloying elements.
- ✓ Excellent mechanical proprieties in the joint area.
- ✓ Fine recrystallized microstructure.
- ✓ Absence of solidification cracking.
- ✓ Process highly automated.
- ✓ Post-FSW formability.
- ✓ FSW can be used to weld similar and dissimilar metals.
- ✓ Weld all aluminium alloys.
- ✓ Replace multiple parts joined by fasteners.

### **Environmental benefits:**

- ✓ No shielding gas required.
- ✓ Minimal surface cleaning required.
- ✓ Eliminated grinding wastes.
- ✓ Eliminated solvents required for degreasing.
- ✓ Consumable materials saving, such as rugs, wire, or any other gases.
- ✓ No harmful emissions.

### **Energy benefits:**

- ✓ Improved material use (e.g., joining different thickness) allow reduction in weight.
- ✓ Only 2.5% of the energy needed for a laser weld.

- ✓ Decreased fuel consumption in lightweight aircraft, automotive, and ship application[2], [4]–[7].

### **Disadvantages:**

- ✗ Limited applications.
- ✗ Low productivity.
- ✗ It creates a visible hole in welding plates.
- ✗ Noisier than other processes.
- ✗ Non-Forgeable material cannot be weld.
- ✗ Thick materials are difficult to weld due to the inhomogeneous heat distribution between the weld upper surface and the lower surface.
- ✗ The heavy-duty fixture is required to hold the workpiece or work during the welding process.
- ✗ Great forces are required to make the pin penetrate the metal.
- ✗ Friction stir welding is not suitable for weld joints where metal deposition is required.
- ✗ The initial investment cost of the friction stir welding machine is very high.
- ✗ Equipment costs are high for conventional facilities.
- ✗ Less flexible than manual and arc welding processes.
- ✗ Limited code inclusion.
- ✗ Process licensing fees.
- ✗ Not easily portable[4]–[7].

## **1.2. DESCRIPTION OF THE PROCESS AND JOINT AREA**

This kind of welding method use a non-consumable rotating tool, with a typical design composed by a pin and a shoulder, that is inserted to the interface of plates or sheet to be joined and advances along the joint line. The principal functions of the tool are three: heating of workpiece, movement of material to produce the joint and containment of hot material under the tool shoulder. The heating, that is localized, is due by plastic deformation of workpiece and friction between the tool and workpiece and induced a softening of material around the pin. This softening combined with tool rotation and translation generate the transition of material from the front of the pin to the back of the pin, thus the space behind the pin fills up and the tool goes forward.

For describing the post-weld microstructure, **Fig. 1.1**, a new nomenclature is required. The first classification was made by Threadgill, and a brief description of different zones is presented:

- *Unaffected material or parent metal*: zone that has not been deformed and that is not affected by the heat because it is far from the weld.
- *Heat-affected zone*: zone in which the material is subject to thermal cycle that has modified the microstructure and/or mechanical proprieties. In this area no plastic deformation occurring.
- *Thermomechanical affected zone (TMAZ)*: zone where heat from the process influences the microstructure and mechanical proprieties and an important deformation is generated due to the high internal friction of the material, caused by the tool movement in the nugget.
- *Weld nugget*: sometimes called also “stir zone”, it is possible observe the fully recrystallized area that refers to the zone previously occupied by the pin[2].

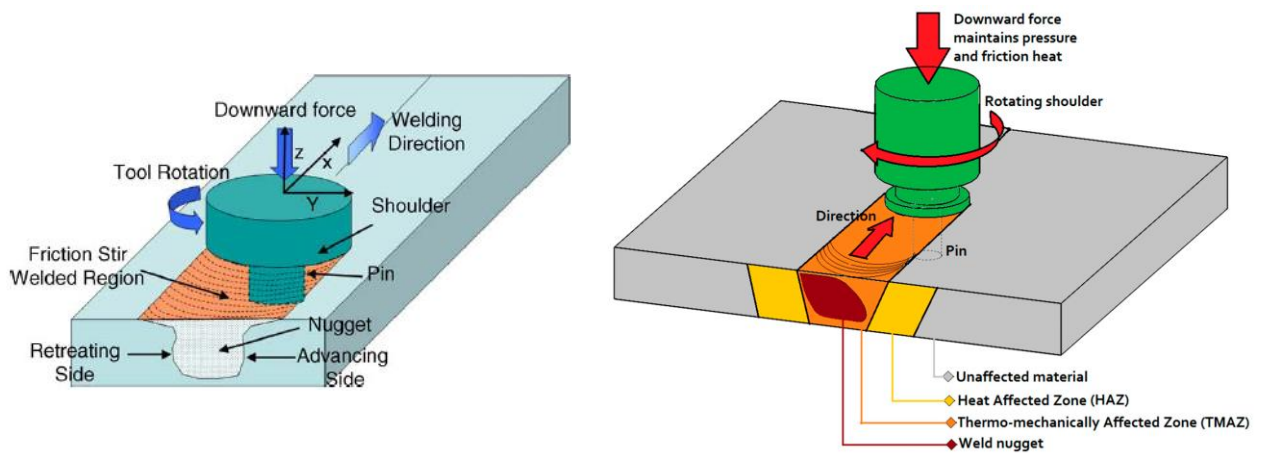


Figure 1.1 On the left schematic drawing of friction stir welding, on the right schematic drawing of joint area[8], [9].

### 1.3. DEFECTS

To obtain a good joint using the FSW a good choice of joint configurations, tool process parameter and a good tool design is required. These measures avoid typical problems that can occur during the welding process, such as the following:

- Void.
- Joint line remnants.
- Root flaws (or incomplete root penetration).

Void formation, **Fig. 1.2**, generally occurs on the feed side of the weld. Given a tool design, the main cause of voids can be low forging pressure, high welding speed, and inadequate clamping of the workpiece. The material deformed by the action of the tool must be able to fill the void generated by the pin. Of fundamental importance is the design of the shoulder of the tool because if it fails to generate enough heat the material will not flow properly and there will be a high probability of the formation of voids. The presence of voids is easily detectable by non-destructive testing methods.

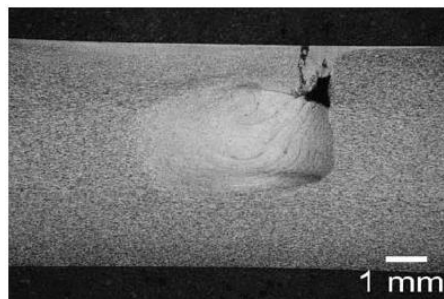


Figure 1.2 Macrograph showing void imperfection in a friction stir welding[10].

A joint line remnant defect, **Fig. 1.3**, (also known as a lazy S, kissing bond, or entrapped oxide defect) is due to the presence of a semi-continuous layer of oxide across the weld nugget. Joint line remnants are formed due to poor cleaning of the surfaces to be joined or insufficient deformation at the interface of the faying surfaces due to improper positioning of the tool with respect to the joining line, a tool shoulder too large, or a welding speed too high.

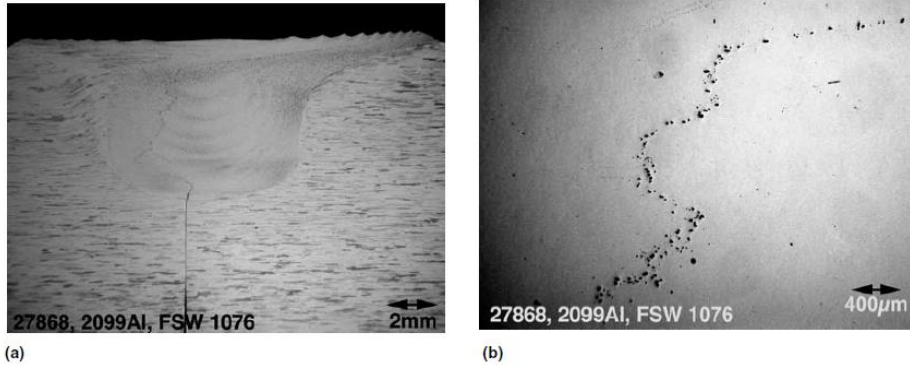


Figure 1.3 Joint line remnant imperfection in a friction stir weld shown by (a) macrograph and (b) magnification of oxide debris that causes the joint line remnant[10].

There are several causes that lead to the formation of incomplete root penetration, **Fig. 1.4**. The main ones are local variations in plate thickness, misalignment of the tool with respect to the joint interface as well as incorrect tool design[10].

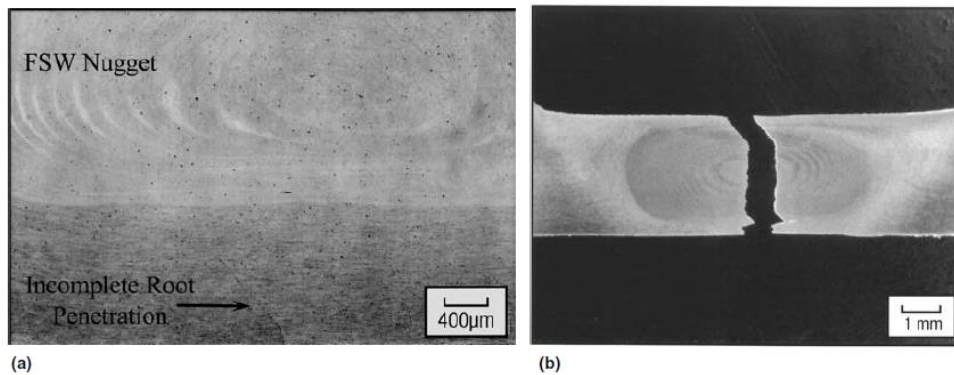


Figure 1.4 Incomplete root penetration imperfection as demonstrated by (a) macrograph and (b) fracture path dictated by incomplete root penetration at the weld root[10].

## 1.4. TYPES OF JOINT CONFIGURATION

There are several kinds of joint configurations for using the technique of FSW, **Fig. 1.5**, the main are square butt, edge butt, T-butt, lap, multiple laps, T-lap, etc. Although, the most convenient configurations are butt and lap joints[11].

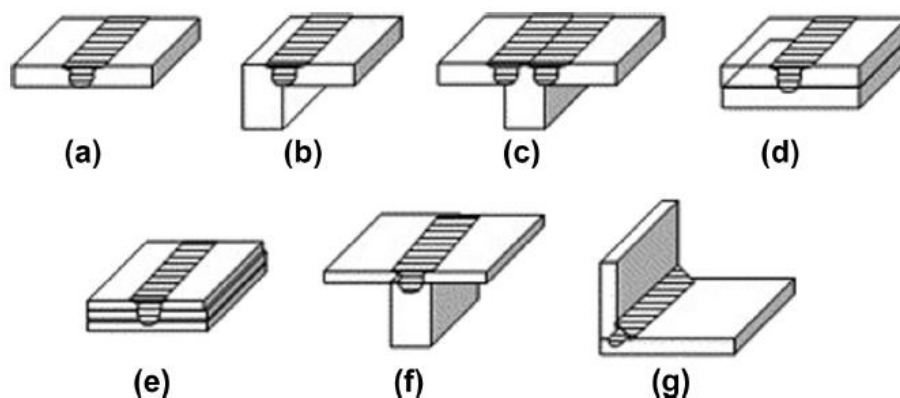


Figure 1.5 Joint configuration for FSW: (a) square butt, (b) edge butt, (c) T butt joint, (d) lap joint, (e) multiple lap joint, (f) T lap joint and (g) fillet joint[2].

Below, in **Fig. 1.6**, some real figures of L-joint and T-joint configurations:

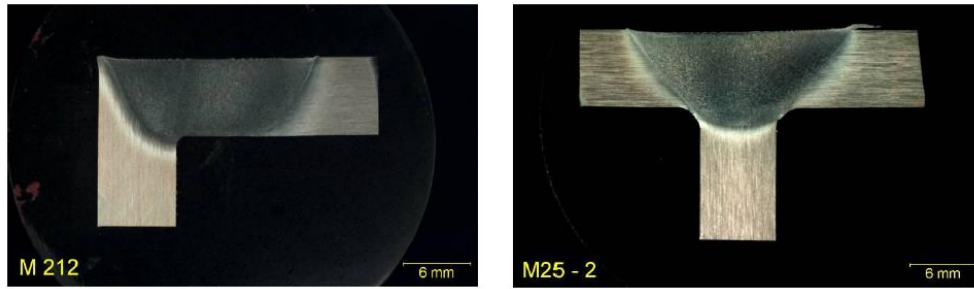


Figure 1.6 On the left the L-joint configuration, on the right the T-joint configuration[12].

An innovative joint configuration is the corner joints. The welding mechanism developed consisted of a rotating pin located in a non-rotating shoulder shaped to the internal corner of the plates to be welded. The shaped shoulder contains the stirred material and slides over the surface of the material during welding. **Fig. 1.7** shows a schematic of the technique applied to a T weld configuration.

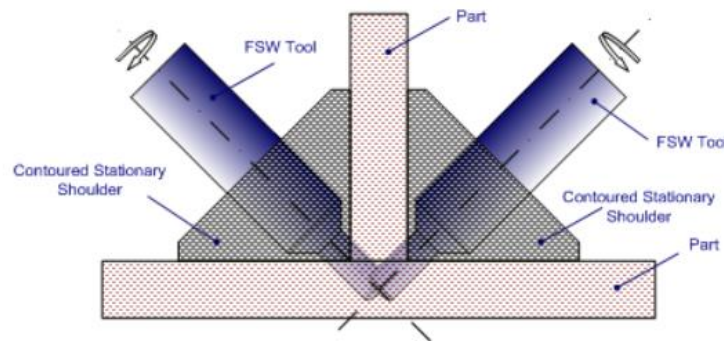


Figure 1.7 Schematic of T weld using corner SSFSW[12].

The samples in **Fig. 1.8** showed all the benefits of the Stationary Shoulder Friction Stir Welding (SSFSW) technique; very smooth weld surfaces, no reduction in cross-section and small heat affected zones however the sharp internal corner was considered detrimental to the joint properties, particularly with regards to joint fatigue susceptibility. The latest developments, particularly in shoulder design, have demonstrated the capability of minimising these stress raisers by forming a fillet radius between abutting plates[12].

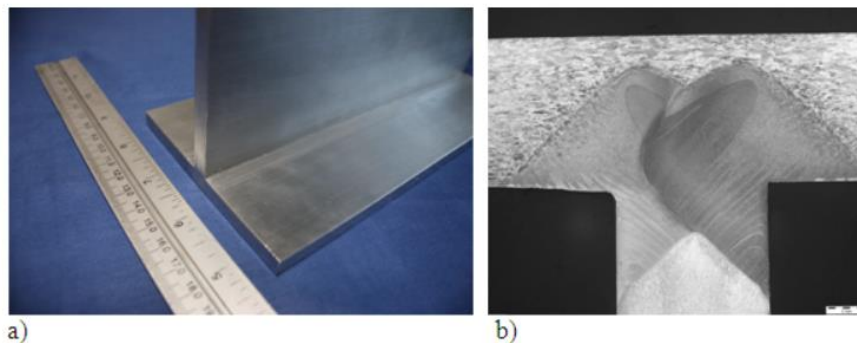


Figure 1.8 A T section fabricated by corner SSFSW in 8 mm thick AA7075-T6 and AA2014-T6: (a) general appearance and (b) macrograph[12].

## 1.5. DESIGN OF TOOL FOR FSW

The design of tool consists in the choice of material of the components of the tool, pin and shoulder, that sometime might be different and the choice of the geometry of previously components. To know the material characteristics of workpiece is very important to decide the material of the tool and to guaranty a long tool life, less wear, and better performance.

The principal tool material characteristics should be:

- **Elevated-Temperature Strength:** the material must be able to resist the compressive loads when the tool impact with the workpiece and have a good compressive and shear strength at high temperature, to prevent the tool distortion or fracture, for all time of welding process.
- **Elevated-Temperature Stability:** during the time of use the tool must maintain dimensional stability and strength.
- **Wear Resistance:** the weld quality might be compromised if there is an excessive tool wear and consequently a change of the tool shape.
- **Tool Reactivity:** the surface proprieties of the tool might change, generally in a negative way, if the tool materials react with the workpiece.
- **Fracture Toughness:** tool fracture toughness influence significantly the phases of tool plunge and dwell. The tool could break due to local stress and strains produced when occurs the first contact with the workpiece.
- **Coefficient of Thermal Expansion:** thermal expansion plays an important role when multi-material tools are used. A huge different of thermal expansion coefficient among pin and shoulder may induce an increment of the stresses and consequently the tool failure.
- **Machinability:** sometime many frictions stir tools require complex mechanical process to make them, any materials that are very difficult to process should not be considered in the tool design.
- **Uniformity in Microstructure and Density:** some inhomogeneities in the microstructure or density produce a major percentage of presence of weak regions within the tool where the fracture may occur.
- **Availability of Material:** the material for producing the tool must be easily available[10].

The pins used in FSW tools produce frictional heating and deformation at the joint surface. It is designed to break the glowing, or contact, surfaces of the workpiece and move the cut material in front of the tool to the rear of the tool[10]. Regarding the geometry, there are several kinds of pin configuration, for example a threaded cylinder, a threaded cylinder with flattened sides, etc.

**Fig. 1.9** shows same tools designed[13].

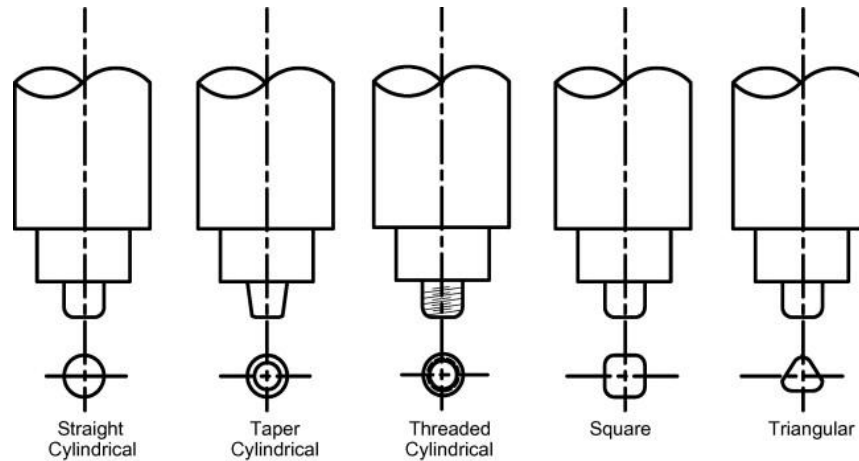


Figure 1.9 Schematic drawing of different typology of pin tool[14].

Tool shoulders are designed to generate heat, through deformation and friction with the material, on the surface and subsurface areas of the workpiece. The shoulder, moreover, through the application of a compressive force performs the downward forging action necessary for weld consolidation. There are different types of tool shoulder geometry, **Fig. 1.10**, the main ones are concave and convex shoulders. The first shoulder design was concave, also commonly referred to as a standard type of shoulder and is currently the most used shoulder type in the FSW. They produce quality welds, and the design is easily machined. The concavity is produced by a small angle between 6 and 10 degrees, between the edge of the shoulder and the pin. Most welds made by FSW with a concave tool shoulder are linear. Early attempts to make and use a convex shoulder were unsuccessful because the convex shape pushed material away from the pin. Tools with convex shoulders have only been made more successfully with the addition of a scroll to the convex shape. The scroll moves the material from outside the shoulder toward the pin. The convex shoulder design allows for more flexibility in the contact area between the shoulder and workpiece, improves the misalignment tolerance of the joint, and allows a technological improvement in the ability to join parts of different thicknesses.

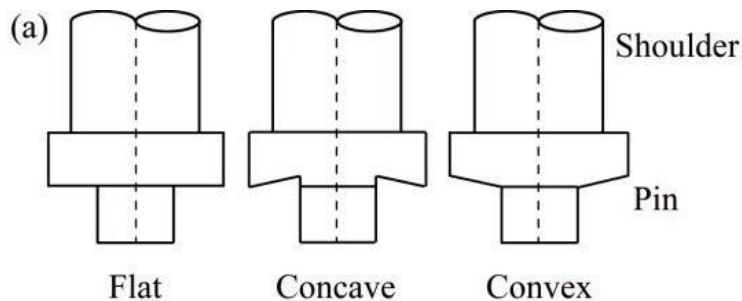


Figure 1.10 Schematic drawing of different typology of shoulder tool[15].

To increase the amount of material deformation, improve part mixing and achieve superior weld quality FSW tool shoulders can contain special features such as scrolls, grooves, ridges or knurls and concentric circles, **Fig. 1.11**[10].

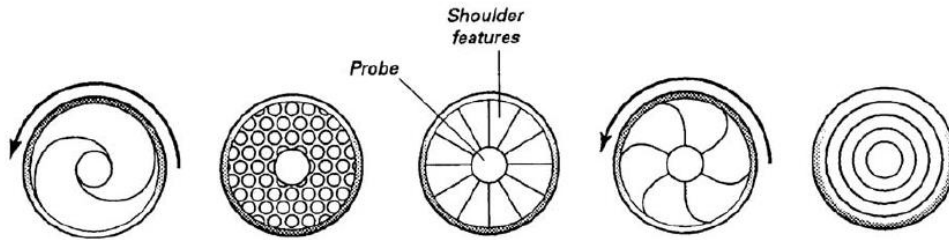


Figure 1.115 Different shoulder features used to improve material flow and shoulder efficiency[10].

## 1.6. TITANIUM AND TITANIUM ALLOYS

Titanium is one of the principal metals presents in the earth's crust with a percentage of 0.6%, therefore it is considered the fourth structural metal in terms of abundance after aluminium, iron, and magnesium. The most relevant mineral sources are rutile ( $\text{TiO}_2$ ) and ilmenite ( $\text{FeTiO}_3$ ), in **Fig. 1.12**.



Figure 1.12 On the left a photograph of rutile, on the right a photograph of ilmenite[16], [17].

A comparison between the basic characteristics of titanium with the other structural metallic materials is showed in the **Fig. 1.13** below.

	Ti	Fe	Ni	Al
Melting Temperature ( $^{\circ}\text{C}$ )	1670	1538	1455	660
Allotropic Transformation ( $^{\circ}\text{C}$ )	$\beta$ $\frac{882}{}$ , $\alpha$	$\gamma$ $\frac{912}{}$ , $\alpha$	-	-
Crystal Structure	bcc $\rightarrow$ hex	fcc $\rightarrow$ bcc	fcc	fcc
Room Temperature E (GPa)	115	215	200	72
Yield Stress Level (MPa)	1000	1000	1000	500
Density ( $\text{g}/\text{cm}^3$ )	4.5	7.9	8.9	2.7
Comparative Corrosion Resistance	Very High	Low	Medium	High
Comparative Reactivity with Oxygen	Very High	Low	Low	High
Comparative Price of Metal	Very High	Low	High	Medium

Figure 1.13 Some important characteristics of titanium and titanium alloys as compared to other structural metallic materials[18].

Observing the **Fig. 1.13** is evident that the titanium has the highest strength to density ratio, nevertheless its application is reduced only for certain niche areas because its price is high. The elevated price is mainly a consequence of the high reactivity of titanium with oxygen that comport the use of vacuum or inert atmosphere during the production process. On the other hand, the high reactivity with oxygen causes the sudden formation of an adherent and stable surface layer when exposed to air, as a result the titanium has a superior corrosion resistance in several kinds of aggressive environments. Titanium is considered, thanks its high melting temperature, the main competitor of aluminium in light weight structural application for high temperature. Pure titanium presents an allotropic phase transformation at 882°C, **Fig. 1.14**, its crystal structure changes from a body-centred cubic ( $\beta$  phase) at higher temperatures to hexagonal close-packed ( $\alpha$  phase) at lower temperatures. The exact transformation temperature is influenced by substitutional and interstitial elements and so depends on the purity of the metal.

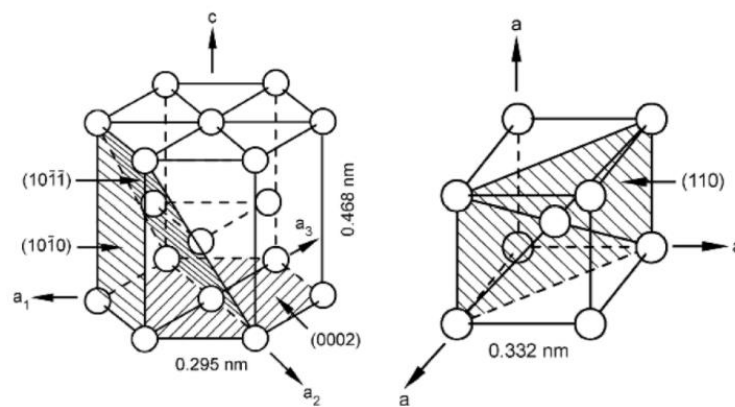


Figure 1.14 On the left unit cell of alpha phase, on the right unit cell of beta phase[18].

Commercial titanium alloys are classified, according to their position in a pseudo-binary section through a  $\beta$ -isomorphous phase diagram **Fig. 1.15**, into three different categories[18]:

- $\alpha$  or near- $\alpha$  alloys
- $\alpha + \beta$  alloys
- $\beta$  alloys

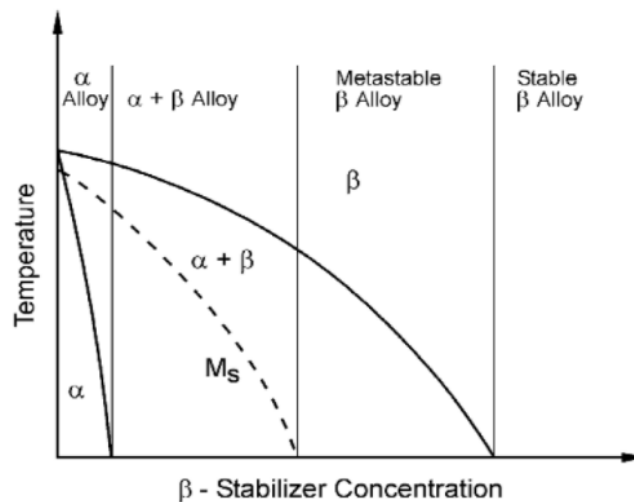


Figure 1.156 Pseudo-binary section through a beta-isomorphous phase diagram (schematically)[18].

The first group of “ $\alpha$  or near-  $\alpha$ ” alloys include the titanium alloys which the annealing is obtain well below the  $\beta$ -transus and present only a small amount of  $\beta$  phase stabilized such as Mo and V (2-5 vol%)[18]. In this category there are two kinds of alloy, the commercially pure grades of titanium and those with intentional addition of  $\alpha$ -stabilizers such as Sn and Al. The first one may be obtained with minimum yield strengths from 170 to 480 MPa, this implies good formability. Other attributes are the excellent corrosion resistance especially in aggressive environments and the good weldability[19].

The second group of “ $\alpha + \beta$ ” alloys have a range in the phase diagram from the  $\alpha / \alpha + \beta$  phase boundary up to the intersection of  $M_s$  line with room temperature[18]. These alloys include Ti-6-4, Ti-6-6-2, Ti-6-2-4-6 and are able of higher strengths than the  $\alpha$  alloys[19].

The group of alloys called “ $\beta$  alloys” are metastable  $\beta$  alloys because they all are in the equilibrium phase region ( $\alpha + \beta$ ) of the phase diagram[18]. These alloys include Ti-10-2-3, Ti-15-3, Ti-13V-11Cr-3Al and are capable of being heat treated to high strengths more than 1380 MPa[19].

A list of the most important commercial alloys belonging to each of three groups is shown below in **Fig. 1.16**.

Common Name	Alloy Composition (wt%)	$T_\beta$ (°C)
<b><math>\alpha</math> Alloys and CP Titanium</b>		
Grade 1	CP-Ti (0.2Fe, 0.18O)	890
Grade 2	CP-Ti (0.3Fe, 0.25O)	915
Grade 3	CP-Ti (0.3Fe, 0.35O)	920
Grade 4	CP-Ti (0.5Fe, 0.40O)	950
Grade 7	Ti-0.2Pd	915
Grade 12	Ti-0.3Mo-0.8Ni	880
Ti-5-2.5	Ti-5Al-2.5Sn	1040
Ti-3-2.5	Ti-3Al-2.5V	935
<b><math>\alpha + \beta</math> Alloys</b>		
Ti-811	Ti-8Al-1V-1Mo	1040
IMI 685	Ti-6Al-5Zr-0.5Mo-0.25Si	1020
IMI 834	Ti-5.8Al-4Sn-3.5Zr-0.5Mo-0.7Nb-0.35Si-0.06C	1045
Ti-6242	Ti-6Al-2Sn-4Zr-2Mo-0.1Si	995
Ti-6-4	Ti-6Al-4V (0.20O)	995
Ti-6-4 ELI	Ti-6Al-4V (0.13O)	975
Ti-662	Ti-6Al-6V-2Sn	945
IMI 550	Ti-4Al-2Sn-4Mo-0.5Si	975
<b><math>\beta</math> Alloys</b>		
Ti-6246	Ti-6Al-2Sn-4Zr-6Mo	940
Ti-17	Ti-5Al-2Sn-2Zr-4Mo-4Cr	890
SP-700	Ti-4.5Al-3V-2Mo-2Fe	900
Beta-CEZ	Ti-5Al-2Sn-2Cr-4Mo-4Zr-1Fe	890
Ti-10-2-3	Ti-10V-2Fe-3Al	800
Beta 21S	Ti-15Mo-2.7Nb-3Al-0.2Si	810
Ti-LCB	Ti-4.5Fe-6.8Mo-1.5Al	810
Ti-15-3	Ti-15V-3Cr-3Al-3Sn	760
Beta C	Ti-3Al-8V-6Cr-4Mo-4Zr	730
B120VCA	Ti-13V-11Cr-3Al	700

Figure 1.16 Important commercial titanium alloys[18].

Titanium and titanium alloys thanks their excellent characteristics find a good application in aerospace applications and sometimes in automotive applications. Below are exposed same considerations about the titanium alloys applications on the base of their microstructure.

#### ***Application of $\alpha$ alloys***

Commercially pure (CP) titanium is used, in the annealed condition, in applications where high formability and corrosion resistance are necessary. Common examples are tubes and pipes in the lavatory system, floor support structure in the galley and lavatory areas, clips and brackets, and ducting for the anti-icing and environmental control system (ECS).

#### ***Application of $\alpha + \beta$ alloys***

The principal representative alloy is Ti-6-4 that includes the 60% of the total titanium production. It is used at a minimum tensile strength of 896 MPa, has a good fracture and fatigue properties and is used in different product forms including bar, casting, forging, foil, sheet, tubing, extrusions, and fasteners. Its properties may be improved through heat treatment like mill anneal, recrystallize anneal and beta anneal.

#### ***Application of $\beta$ alloys***

The most significant representative alloy is Ti-13V-11Cr-3Al, it was used widely on the SR-71 “Blackbird” reconnaissance airplane. About 95% of the structural weight was reported to be titanium, majority of components like wing and body skins, longerons, frames, ribs, bulkheads, rivets, and gear are made with Ti-13V-11Cr-3Al. The main reason of this material choice is its thermal stability[19].

## 2. FSW OF TITANIUM

In the aerospace engineering titanium is the most emerging usable metal so the necessity of use welding process to join different components is mandatory. Especially the welding parameters play an important role in welding process which reflects in microstructural changes in the Fusion Zone and Heat Affecting Zone. The main kinds of welding process that may be used for joining the titanium workpieces are the following:

- TIG and Plasma welding process.
- Laser welding.
- Friction Stir Welding.
- Hybrid Techniques in the welding process[20].

Fusion welding techniques such as laser welding or TIG welding are widely used to join titanium alloy sheets. However, the formation of a brittle weld, unwanted deformation, and the presence of residual stresses limit their application to critical structural components[21].

In this thesis work the study and research are focused on the friction stir welding process applied to sheet of pure titanium in lap joint configuration.

### 2.1. DEFECTS IN TITANIUM JOINTS

The presence of defects in welds made with FSW technology on titanium or titanium alloy sheets are in most cases the result of an incorrect choice of material and tool geometry or an incorrect setting of process parameters such as: tool rotation speed, tool feed speed, sink rate, plunge depth and tilt angle. **Fig. 2.1** shows the relationship between welding parameters and welding defects obtained from the studies of H. Liu et al. by performing FSLW tests under load control. It can be observed that groove-like defect was found when welding was performed with high welding speeds (or low rotational speeds) and consequently there was insufficient heat input. By decreasing the welding speed and maintaining the same rotation speed (or increasing the rotation speed while maintaining the same welding speed), the groove-like defect disappears, and the inner cavity defect appears. With proper heat input, the defect-free joint was made with a rotation speed of 250 rpm and a welding speed of 75 mm/min. With a further decrease in welding speed (or an increase in rotational speed), the overheating rough surface and tool penetration defects were formed due to excessive heat input.

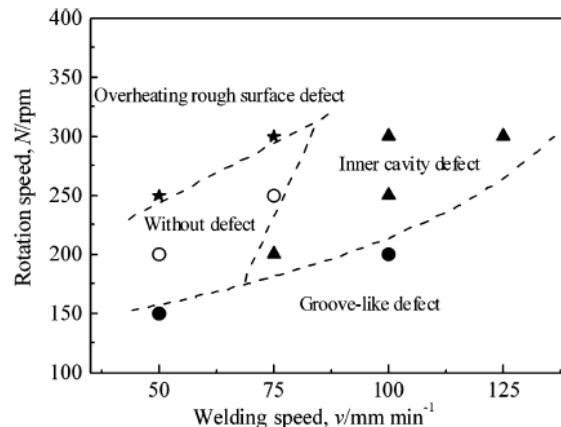


Figure 2.1 Relationship between welding parameters and welding defects under tool load control/[1].

The cross sections and surface appearance of the defects are shown in **Fig. 2.2**. The groove-like defect was found in the retreating side (RS) of the stirring zone (SZ) and the inner cavity defect was found in the middle part of the SZ[1].

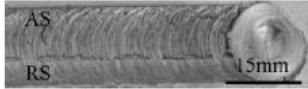
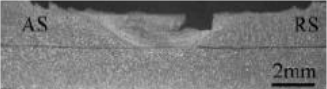
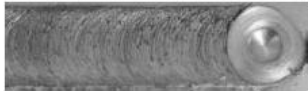
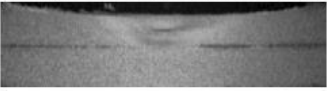
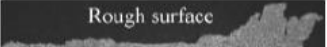
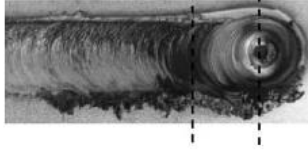
Heat input	Average $N/V$ , $\text{mm}^{-1}$	Welding defect	Surface appearance	Cross-section
Insufficient	2·2	Groove-like defect		
	2·7	Inner cavity defect		
Excessive	4·2	Overheating rough surface and tool penetration defect		
				

Figure 2.2 Surface appearances and cross-sections of welding defects under tool load control[1].

In another study by Shude Ji and Zhengwei Li, the key process parameters for reducing the occurrence of the hook defect within welds of Ti-6Al-4V sheets placed in the lap configuration are highlighted. The results obtained are as follows.

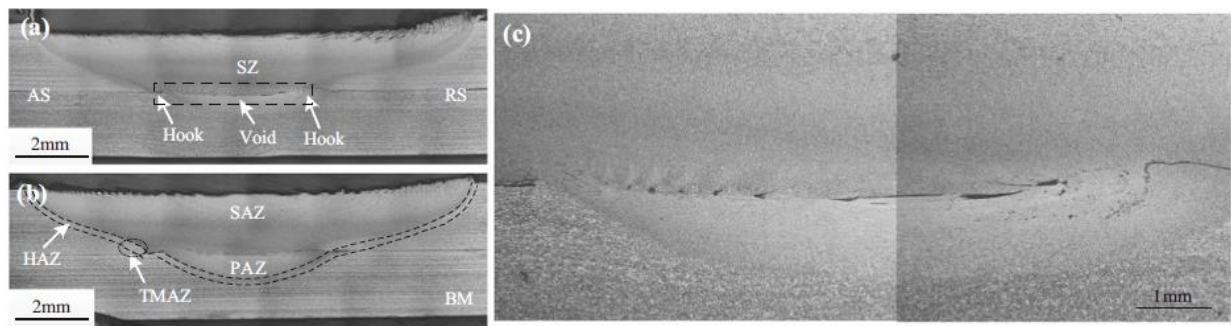


Figure 2.3 Cross sections and defect of the joints: (a) 180 rpm, (b) 150 rpm and defect (c)[22].

**Fig. 2.3(a)-(b)** shows cross sections of joints made using different tool speeds. At advancing side (AS), very small hooks can be observed on both joints. At retreating side (RS), both hooks show rather flat morphologies. Thus, it is included that the hook can be reduced when the pin slightly penetrates the bottom sheet. In **Fig. 2.3(c)**, a void-like defect near the original interface between the plates near the stir zone (SZ) is observed in the lower part of the joint made at 180 rpm.

Although Su et al.[23] and Mironov et al.[24] attributed the defect to insufficient material flow in the pin tip region, in the present study by Shude Ji and Zhengwei Li show that the defect can be avoided by lowering the tool rotation speeds to 150 rpm. **Fig. 2.4** shows the magnified views of the hooks using different rotating speeds[22].

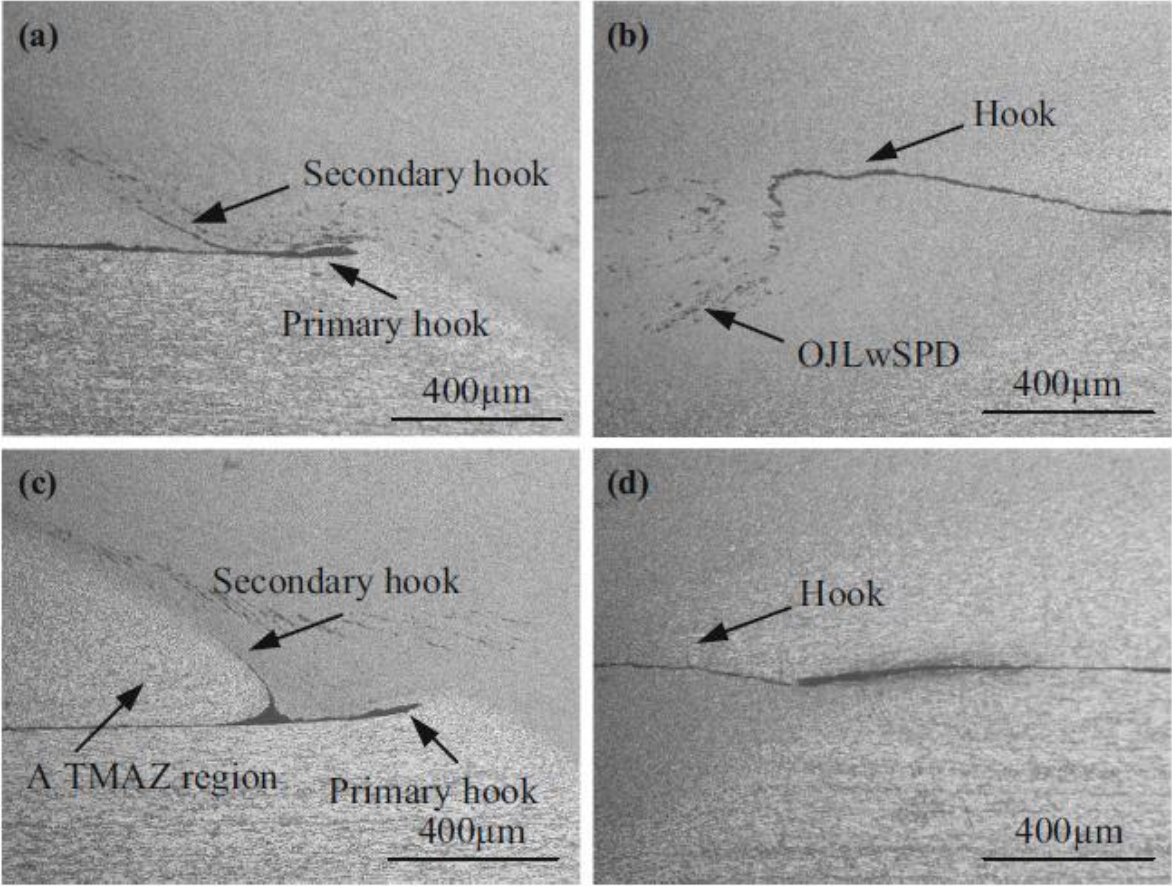


Figure 2.4 Hooks using different rotating speed: (a) and (b) hooks of AS and RS using 180 rpm, (c) and (d) hooks of AS and RS using 150 rpm[22].

## 2.2. FSW OF COMMERCIAL PURE TITANIUM IN LAP AND BUTT JOINT CONFIGURATION

One of the few studies carried out on the FSW process applied to pure titanium were by H. Liu et al., they analysed the effects of welding parameters on the microstructural characteristics of the joint. The material used in this research was a pure titanium sheet with dimensions of 300 x 100 x 2 mm, with a chemical composition of Ti-0.01C-0.03Fe-0.01N-0.1O-0.001H (wt-%), **Fig. 2.5**. FSW of the joint was performed in both tool load control and dip depth control using a tool made from WC-Co. The tool dimensions were 15 mm and 6 mm in shoulder and pin diameter, respectively, and with a pin length of 2 mm. The axial force was set to 14.7 kN under tool load control. Depth of immersion control was achieved by changing the axial force on the tool during FSW, which means that the axial force was reduced (or increased) automatically as the depth of immersion increased (or decreased). The rotational speeds were set from 200 to 350 rpm and the welding speeds from 50 to 150 mm/min.

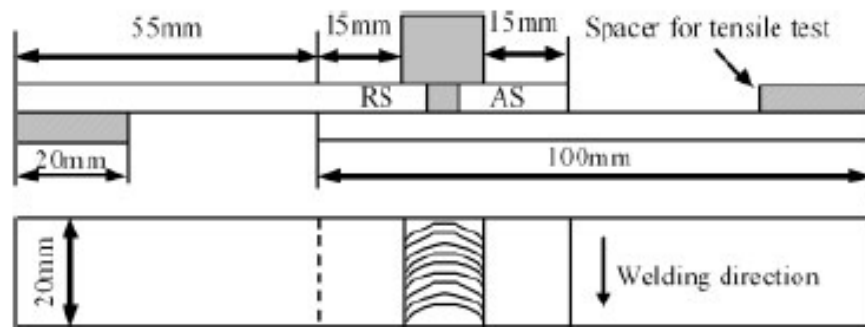


Figure 2.5 Relative position of pure titanium lap joint for lap shear strength test[1].

Based on the experiments in tool load control, they concluded that the lap width strongly influences the breaking load. Consequently, to increase the breaking load, the lap width must be increased by increasing the axial force, but this leads to an easy overheating of the contact surfaces which may lead to the formation of penetration defects. Joints without defects have been realized with tests in immersion depth control at 250 rpm, 75 mm/min and 200 rpm, 50 mm/min with lap widths up to 4.5 mm, reaching breaking loads of 14.5 kN as shown in the **Fig. 2.6** below.

Control system	Rotational speed, rev min <sup>-1</sup>	Welding speed, mm min <sup>-1</sup>	Macrostructure	Lap width, mm	Failure load, kN
Load control					
Plunge depth control	250	75		2.7	11.9
	200	50		4.5	14.5
	250	75		4.5	14.4

Figure 2.6 Welding parameters, macrostructures, lap widths and failure loads of joints without defect under conditions of tool load or plunge depth control[1].

The tensile curves obtained by the investigators are shown in **Fig. 2.7** below.

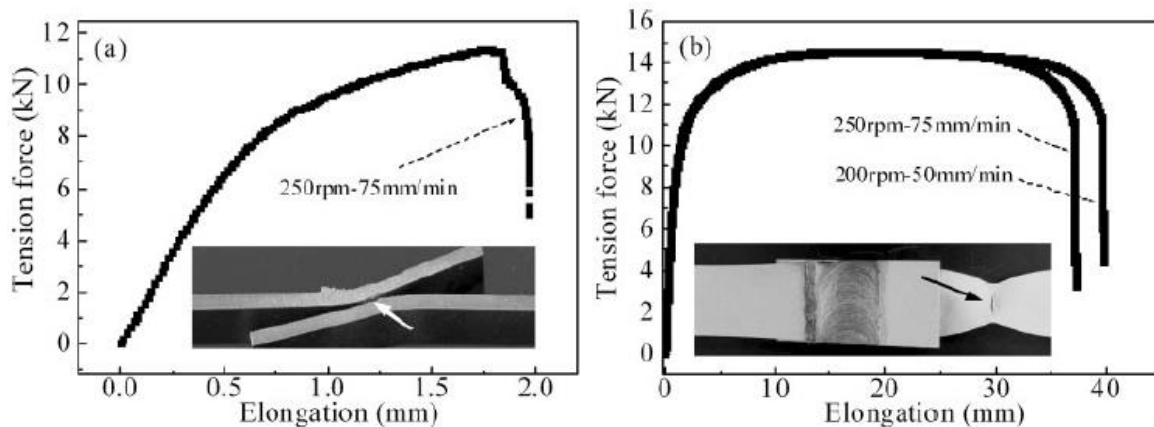


Figure 2.7 Tensile curves of joint without defect under conditions of tool, (a) load control and (b) plunge depth control[1].

The tensile curves rise rapidly at the beginning of the tensile test, approximately flatten out in the middle, and then decrease sharply at the end. A good lap width provided sufficient bond strength to lead to fracture of the base metal after large elongation[1].

Based on previous studies, the research group of H. Liu et al. continued studies on the fabrication of a good-quality joint between two pure titanium sheets using the FSLW solid-state welding process. The material used to fabricate the joint is a grade 2 titanium alloy with chemical composition of Ti-0.01C-0.03Fe-0.01N-0.1O-0.001H (mass-%). The tool used is inclined 3 degrees from vertical and was obtained by WC-Co sintering processes.

A schematic of the pin is shown in **Fig. 2.8** below.

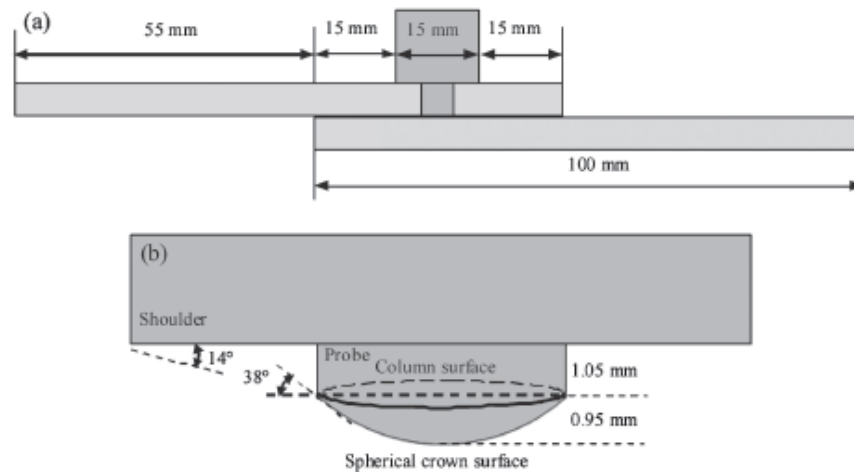


Figure 2.8 Schematic illustrations of: (a) the pure titanium lap joint and (b) the probe shape[25].

A plunge position control with a plunge depth of 2.3 mm and a vertical force of 19.6 kN was used during the FSLW process. The rotational speed was varied from 150 to 300 rpm instead the welding speed was adjusted from 50 to 125 mm/min. The optimal conditions of the process parameters for obtaining a good weld are given in **Fig. 2.6**, defect-free joints are obtained with a rotation speed of 250 rpm and welding speed of 75 mm/min or with a rotation speed of 200 rpm and feed speed of 50 mm/min.

EBSD (electron backscattered diffraction) maps **Fig. 2.9** were made in various regions of the joint made with rotation speed of 250 rpm and welding speed of 75 mm/min along with a low magnification view of the joint cross section. The grains in the EBSD maps are coloured in terms of crystal direction relative to the welding direction (WD). It can be seen from the overview that the joint was composed of the base metal (BM), the thermomechanical zone (TMAZ), and the stirring zone (SZ). The titanium plates are held together by a zone defined as the lap zone (LZ) shown in the overview. It can also be seen that the shape of the SZ is influenced by the geometric shape of the welding tool. The BM is characterized by coarse grains, while the microstructure in the SZ is depicted with finely ordered grains. The grain structure of the SZ is the result of recrystallization due to the action of heavy plastic deformation and a relatively high temperature.

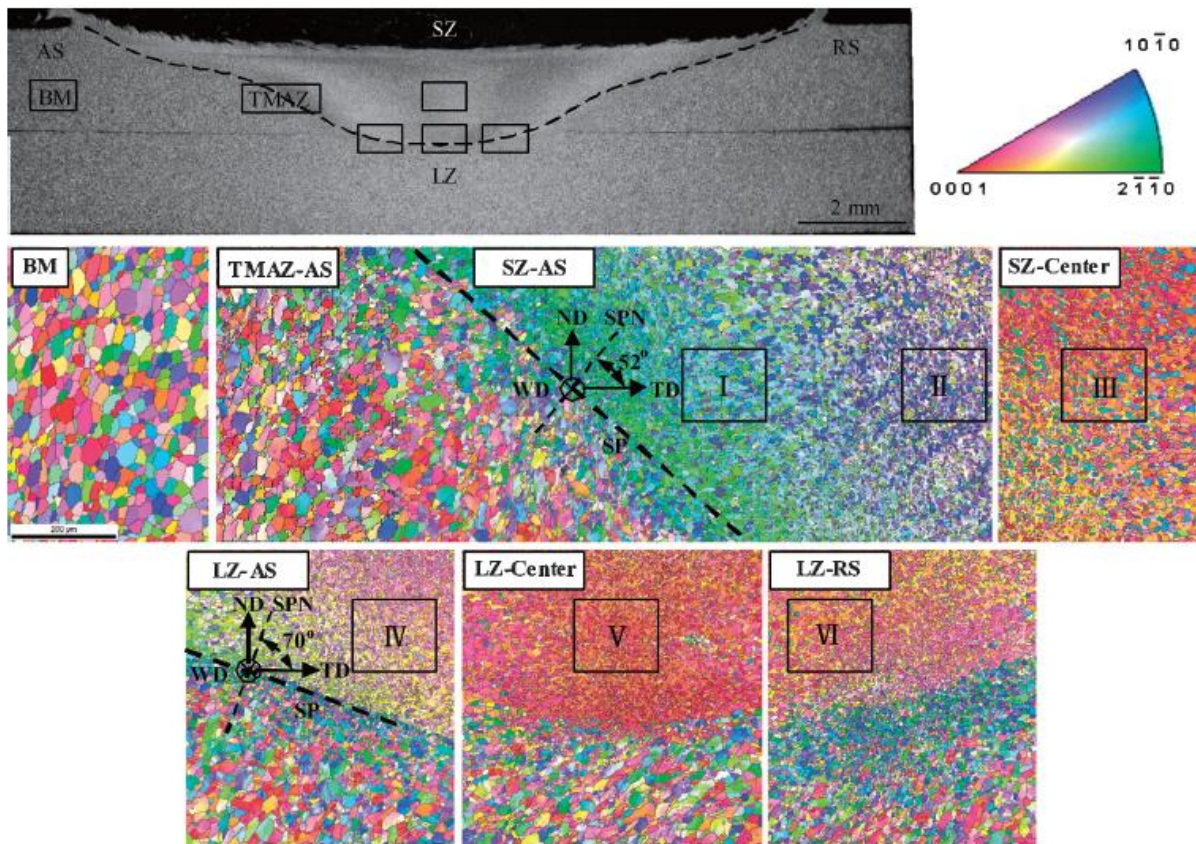


Figure 2.9 A low magnification overview of the cross-section of the lap joint at 250 rpm and 75 mm/min and EBSD maps in various regions of the joint[25].

Captions:

- AS: advancing side
- RS: retreating side
- WD: welding direction
- TD: transverse direction
- ND: normal direction

Below are the hardness profiles, **Fig. 2.10**, in the joint made with a rotation speed of 250 rpm and welding speed of 75 mm/min both along the horizontal direction (dashed black line) and along the vertical direction (dashed white line). The hardness distribution is somewhat scattered but the average hardness value in the SZ is significantly higher than that in the BM. **Fig. 2.11** gives the average grain size and hardness in the BM and SZ as well as the fracture load and fracture location of the tensile specimen. The fracture location in the BM is likely attributed to two aspects, the increased hardness in the SZ resulting in increased strength in the SZ compared to the BM, and the sufficient width of the LZ providing sufficient bond strength and thus preventing fracture in the LZ[25].

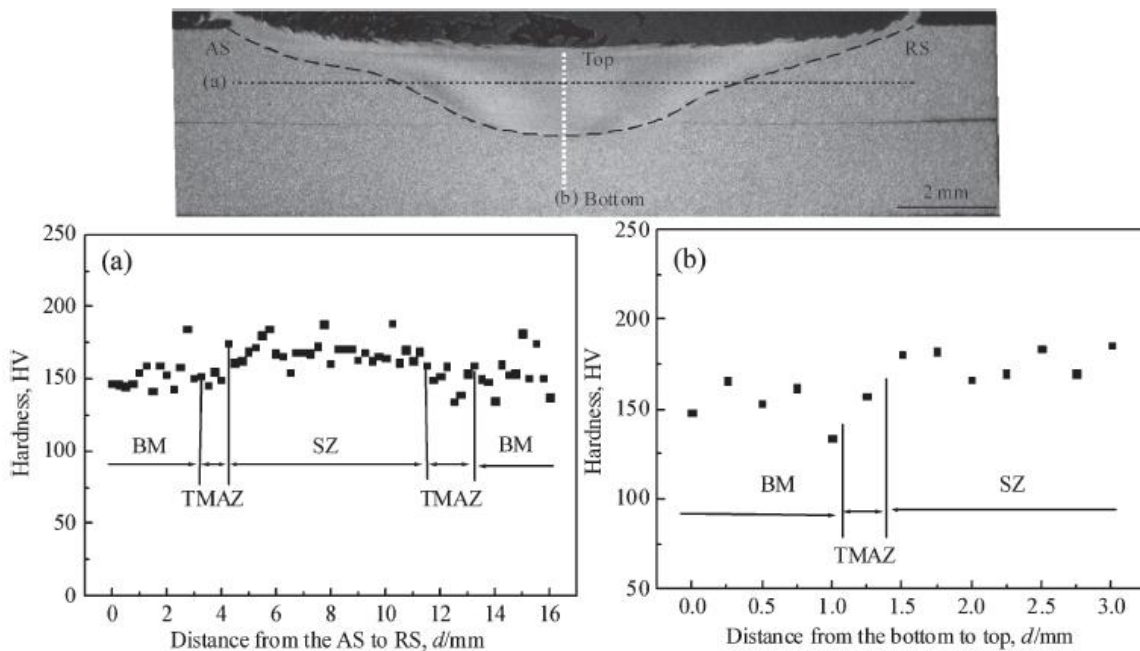


Figure 2.10 Above the grain orientation and texture evolution in pure titanium lap joint produced by FSW. Hardness profiles in the lap joint along: (a) the horizontal direction from the AS to RS; (b) the vertical direction from the bottom to top[25].

Grain size in the BM ( $\mu\text{m}$ )	Grain size in the SZ ( $\mu\text{m}$ )	Hardness in the BM ( $H_V$ )	Hardness in the SZ ( $H_V$ )	Average failure load (kN)	Fracture location
22	6	153	173	14.5	BM

Figure 2.11 Grain size, hardness, average failure load and fracture position of the lap joint[25].

The same team led by H. Liu continues the studies on FSW applied to commercially pure titanium and in another paper, they discuss the results obtained from the joining of 2 mm thick plates obtained with the use of 3 tools of the same material, sintered WC-Co, but with different dimensions, **Fig. 2.12**. The shoulder of the tools remains for all of them 15 mm in diameter instead the pin has the same diameter, 6 mm, for all the tools but different lengths of 1.8, 2.0 and 2.2 mm respectively. The tests were conducted with a load control system with a penetration force of 14.7 kN. The rotational speeds were modulated from 200 to 400 rpm, and the welding feed rates were varied between 60 and 200 mm/min. After welding, the joint was sectioned, polished, and

chemically attacked with a solution of hydrofluoric acid, nitric acid, and distilled water in a 1:1:8 ratio, finally examined under an optical microscope. Following metallographic analysis, shear strength tests were performed using a tensile testing machine at room temperature and a crosshead speed of 1 mm/min.

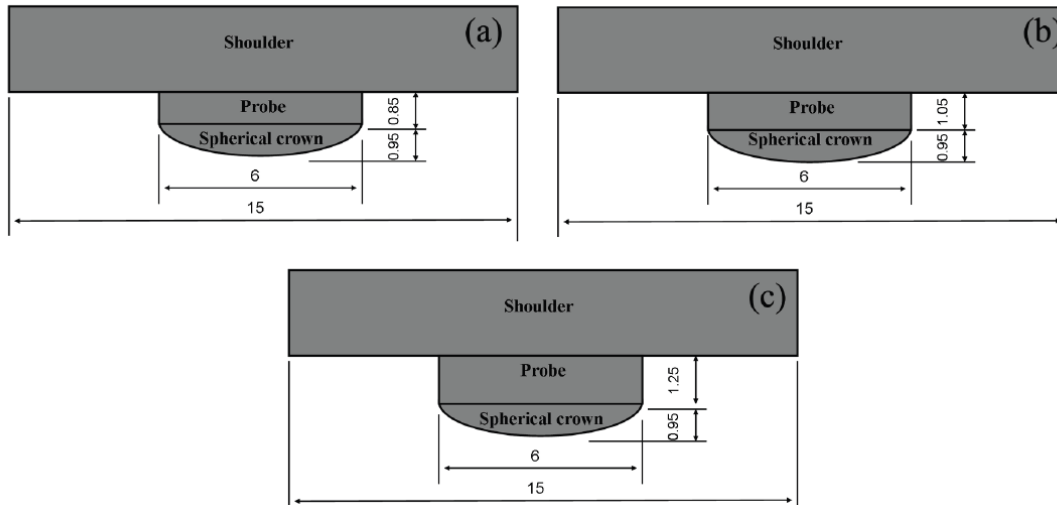


Figure 2.12 Schematic illustration of the FSW tools with probes of: (a) 1.8 mm, (b) 2.0 mm and (c) 2.2 mm in length[26].7

Fig. 2.13 shows the influence of process parameters on the occurrence of typical welding defects.

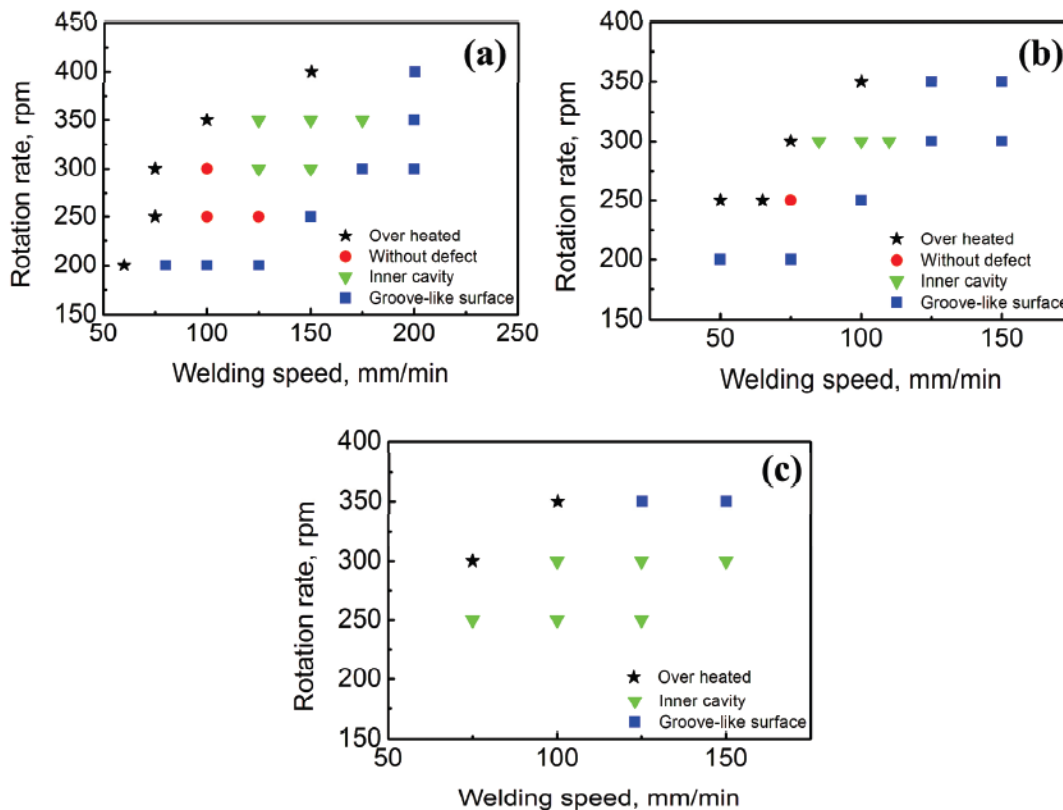
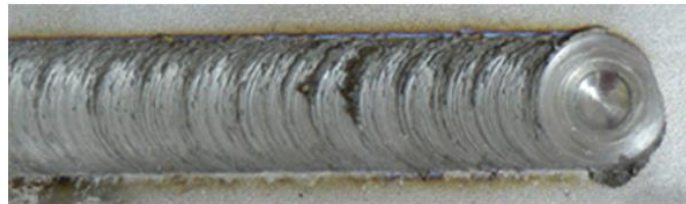


Figure 2.13 Relationship between welding parameters and welding defects for the lap joints welded using probes with lengths of (a) 1.8 mm, (b) 2.0 mm, and (c) 2.2 mm[26].



**(a) Overheating and tool penetration defect**



**(b) Sound surface appearance**



**(c) Groove-like defect**

*Figure 2.14 Fig. 4. Typical surface appearances of the pure titanium lap joint processed using 2.0 mm probe at (a) 350 rpm, 100 mm/min, (b) 300 rpm, 100 mm/min, and (c) 350 rpm, 150 mm/min[26].*

The rough surface overheating defect along with the tool penetration defect are shown in **Fig. 2.14 (a)**. Both defects appeared when welding occurred at low feed rates or at high tool rotation speeds. This is explained by the fact that the high heat input accelerated the phase transformation of alpha phase to beta phase during FSW. A typical groove-like defect can be observed in **Fig. 2.14 (c)**, the defect occurs when feed rates are high, or tool rotation speeds are too low. It is associated with low heat input and consequently insufficient material flow. A properly made joint can be seen in **Fig. 2.14 (b)** and was obtained with the following combinations of process parameters:

Tool with pin length equal to 1.8 mm

- 300 rpm - 100 mm/min
- 250 rpm - 100 mm/min
- 250 rpm - 125 mm/min

Tool with a pin length of 2.0 mm

- 250 rpm - 75 mm/min

Very interestingly, the 2.2 mm pin length tool narrowed the range of optimal process parameters so much that it was unable to produce a quality splice.

From the analysis of the tensile test results, it can be observed, in **Fig. 2.15**, that the junction made by FSW provided sufficient bond strength in the nugget zone, which led to the fracture of the base metal after large elongation. Electron backscatter diffraction (EBSD) examination showed that the

microstructure in the nugget zone is different from that of the base metal (BM). The BM is characterized by coarse grains, whereas the microstructure in the stirring zone is characterized by fine grains. The fine grain structure is assumed to be the result of dynamic recrystallization due to strong plastic deformation at relatively high temperature. The reason why the fracture position of the shear tensile specimen was at the BM is probably attributed to two aspects:

- Hardness is increased in the stirring zone.
- Adequate weld size provides sufficient bond strength to prevent fracture in the nugget zone[26].

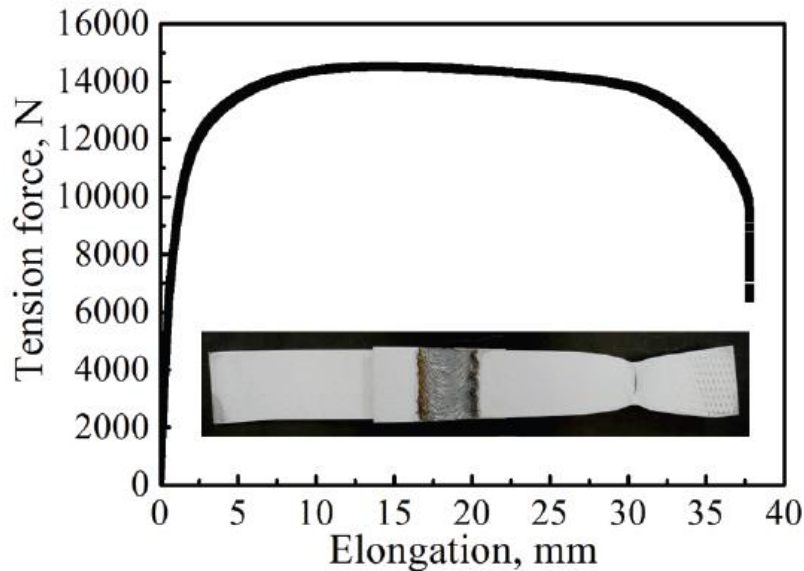


Figure 2.15 Tensile curves of CP Ti lap joint processed at 250 rpm, 75 mm/min using probe with lengths of 2.0 mm[26].

Other experiments were developed by Hidetoshi Fujii. Commercially pure titanium plates with dimensions of 300×50×2 mm was welded in butt configuration under load control. The chemical composition of commercially pure Ti is 0.007C-0.0013B-0.08O-0.004N-0.05Fe (in wt.%). Tungsten carbide-based alloy tools with respective dimensions were used for FSW processes:

- Shoulder of 14 mm in diameter.
- Pin of 6 mm in diameter.
- Pin length of 1.8 mm.

The rotational speed of the tool is set at 200 rpm, and the welding speed is modulated from 50 to 300 mm/min. During welding, a protective atmosphere of Ar gas flows around the tool to prevent oxidation of the joints. Following joint fabrication, the weld section was observed by light microscopy and then by backscatter electron diffraction (EBSD) and transmission electron microscopy (TEM). After metallographic analysis, tensile tests performed at a crosshead speed of 1 mm/min were also performed. Vickers micro-hardness analysis was obtained under a load of 0.98N for a dwell time of 15 s along the centrelines of the cross-section with an interval of 0.5mm.

**Fig. 2.16** shows the peak temperature measured in the stirring zone of welds processed at different welding speeds. The graph shows that the maximum temperature during the welding process can reach 843, 694, 555, and 498 °C at a welding speed of 50, 100, 200, and 300 mm/min, respectively.

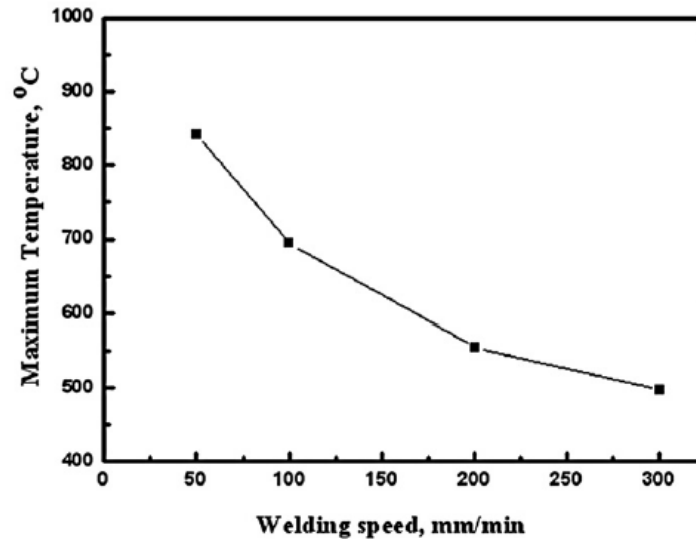


Figure 2.16 Peak temperature measured in the stir zone welded at different welding speeds[27].

This indicates that all joints were processed below the phase transformation temperature. In addition, the parts were exposed to high temperature for a very short time because of the rapid movement of the rotating tools; therefore, it is believed that no phase transformation occurred under all these welding conditions. **Fig. 2.17** shows the Vickers micro-hardness analysis, where the broken line indicates the hardness of the base metal. The hardness in the stirring zone increases with increasing welding speed.

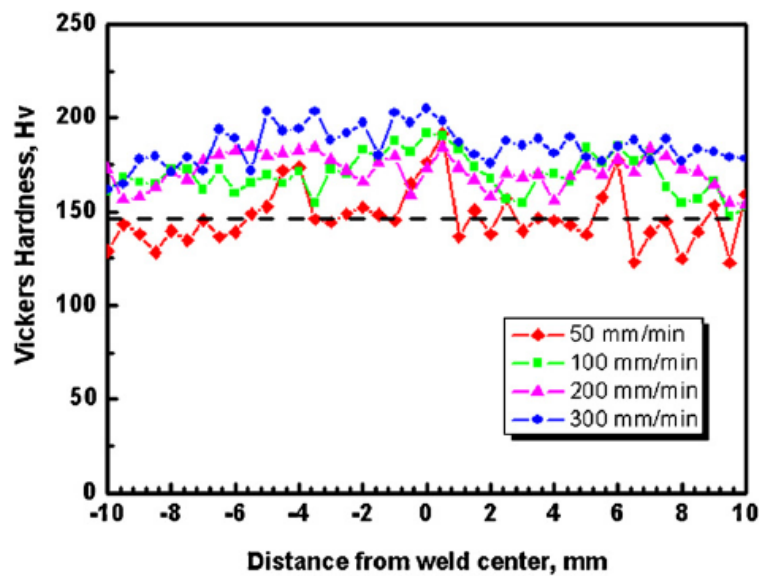


Figure 2.17 Hardness profile in the stir zone welded at 50, 100, 200 and 300 mm/min, together with the hardness of the base metals[27].

**Fig. 2.18** shows the tensile strength of machined joints at different welding speeds. The tensile strength of the base metals is about 420MPa (indicated by a dotted line in the figure). For specimens obtained at a feed rate of less than 200 mm/min, fracture occurred in the stirring zone indicating that the weld strength is lower than that of the base metal. However, the tensile strength increased with increasing feed rate due to the refinement of the microstructure. At weld feed rates of 200 mm/min, the tensile strength of the joint exceeds that of the base metal; as a result, the specimen has fractured into the base metal. However, when the welding speed is increased to 300 mm/min, the tensile strength of the specimens again decreases despite the significant refinement of the microstructure, this is due to the formation of weld defects in the stirring zone[27].

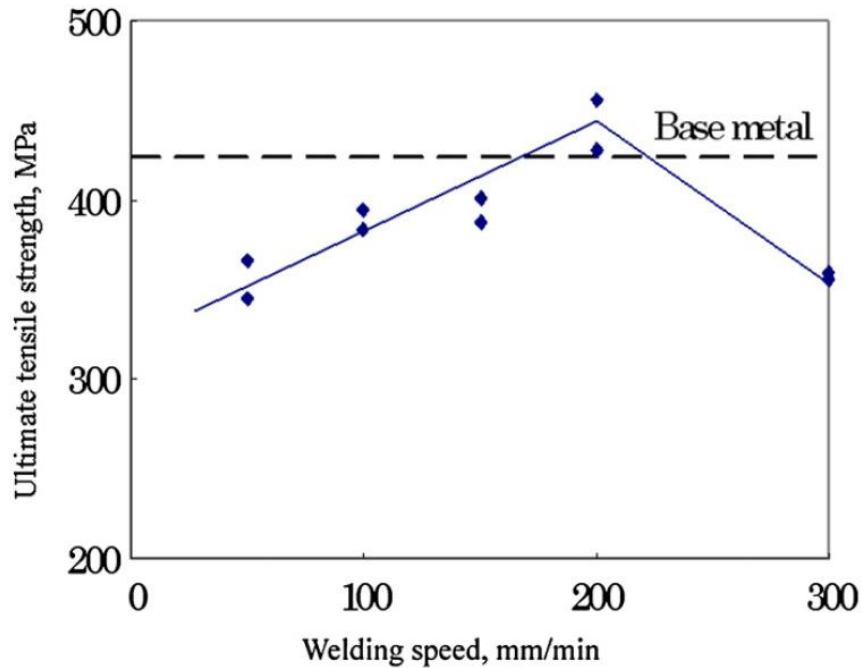


Figure 2.18 Tensile strength of the samples at different welding speeds, together with that of the base metal[27].

Another interesting research was carried out by Won-Bae Lee et. Al., commercially pure titanium sheets with a thickness of 5.6 mm were joined using the FSW technique. The tool used is TiC, obtained by sintering process, is cooled with a water-cooling system. The process parameters used for making the joint are:

- Tool rotation speed equal to 1100 rpm.
- Welding feed rate of 500 mm/min.

**Fig. 2.19** shows the upper (a) and lower (b) surfaces of the weld.

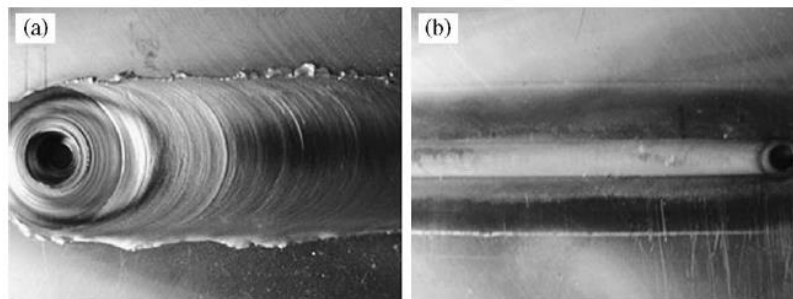


Figure 2.19 Surface images of friction stir welded Ti: (a) upper surface and (b) rear surface[28].

No surface welding defects were observed under these FSW machine setting conditions. Next, the specimen is sectioned and polished, chemically attacked with a solution consisting of HF (5ml), HNO<sub>3</sub> (5ml), and H<sub>2</sub>O (70ml), and prepared for optical microscope (OM) and transmission electron microscope (TEM) analysis. Then, the specimen is subjected to micro-hardness test with a load of 300g for 10 s, and tensile test using a head speed of 1mm/min.

**Fig. 2.20** shows the optical macrostructure and microstructures of the weld zone. The optical observation of the macrostructure reveals that the FSW of the Ti plates was successful judging by the fact that no weld defects are seen in the weld zone.

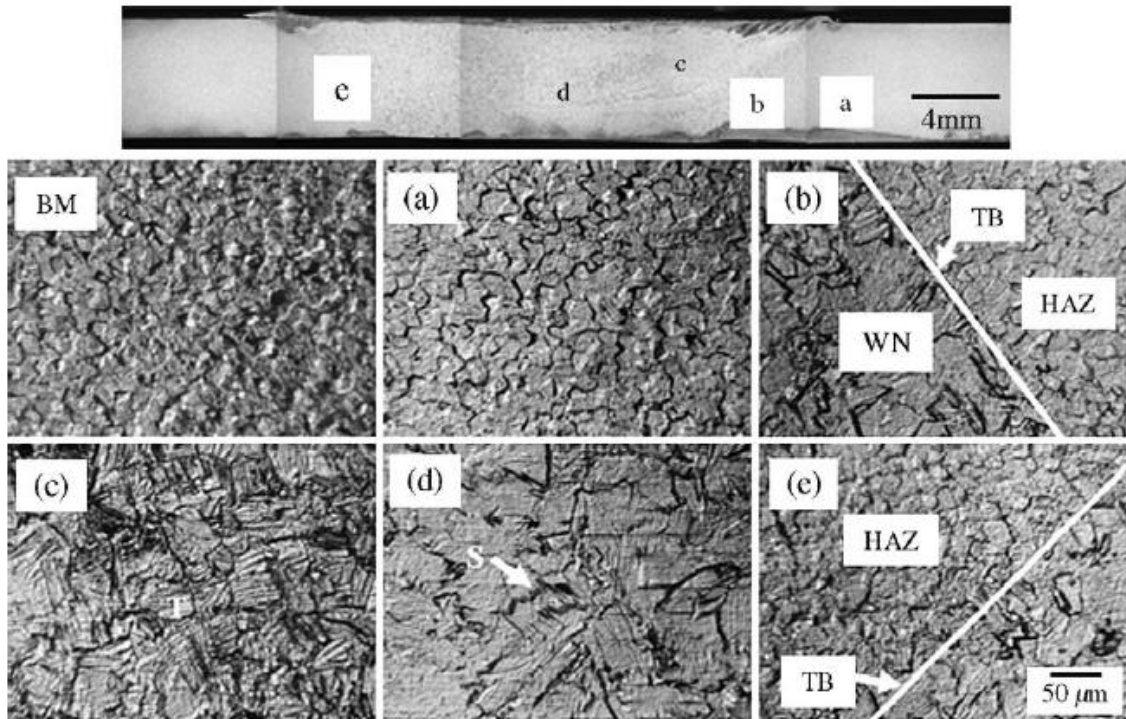


Figure 2.20 Optical macrostructure and microstructures: (a) HAZ, (b) TB on advancing side, (c) WZ in upper middle part, (d) WZ in central part and (e) TB on retreating side[28].

- BM: Base material
- WN: Weld nugget
- HAZ: Heat affected zone
- TB: Transition boundary

**Fig. 2.21** shows the hardness distribution near the weld zone in the direction marked by the dashed line in the macro-image. The hardness in the weld nugget (WN) has scattered values, with an average hardness like that of the base material (BM).

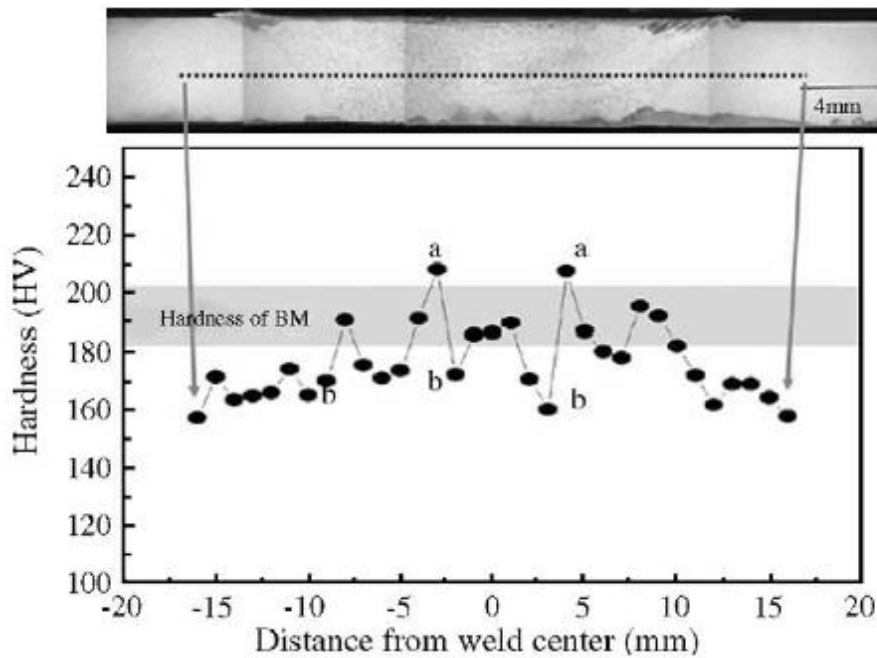


Figure 2.21 Cross-sectional hardness distribution near the weld zone[28].

**Fig. 2.22** shows the tensile test results and the fractured specimens. The transverse tensile strength of the joint shows an average of 429 MPa which is slightly lower than that (440 MPa) of Ti BM because the fracture occurred in the part of the HAZ with minimum hardness. It is noted that the fractures occur only in the HAZ on the shrinkage side and not on the advance side[28].

	Joint 1	Joint 2	Average	Base metal
Tensile strength (MPa)	433	426	430	440
Elongation (%)	21	19	20	25

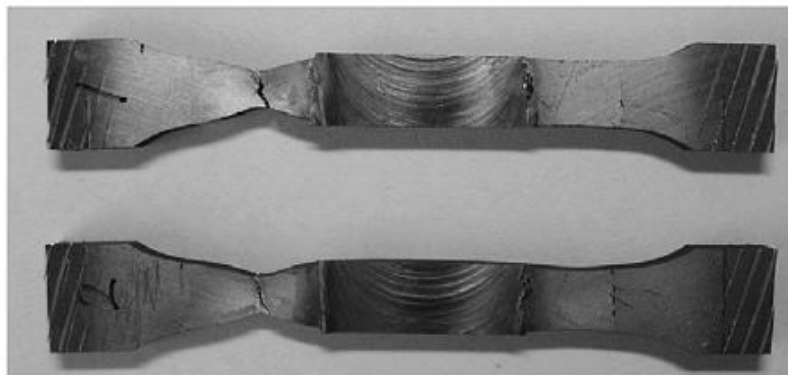


Figure 2.22 Results of tensile test and photos of fractured specimen after tensile test[28].

### 2.3. DESIGN OF TOOL FOR FSW OF TITANIUM

The high mechanical strength and low thermal conductivity of titanium cause very high frictional forces and heat generation at the interface between tool and workpiece, thus limiting the possible materials that can be used to make tools for FSW. In the case of other alloys such as Al and Mg, due to their low strength and low melting point, the tool is made from steel[21].

Particularly the premature wear and the failure of tool must be avoided. A study carried out by I.K.Chernykh et al. shows experimentally that the wear of a steel tool used to weld two titanium sheets, using the FSW technique, occurs early without producing acceptable results from the point of view of the welded joint. First, the goal of the experiment is to be able to join two 1.8 mm thick titanium alloy sheets (OT-4 and VT-20) in a butt configuration using a steel tool (1.2343X37CrMoV5-1).

Tests are performed on two specimens with the following process parameters, 80 rpm tool rotation speed and 16 mm/min feed rate for the first specimen and 160 rpm and 25 mm/min for the second specimen. The **Fig. 2.23** below shows the progress of steel tool wear.



Figure 2.23 The destruction of the pin of the tool from 4H5MFS steel[29].

During welding, the pin of the tool melted and destroyed. This indicates an insufficient heat resistance of a tool made of 1.2343X37CrMoV5-1 for FSW of titanium alloys. The specimens are shown in **Fig. 2.24**.

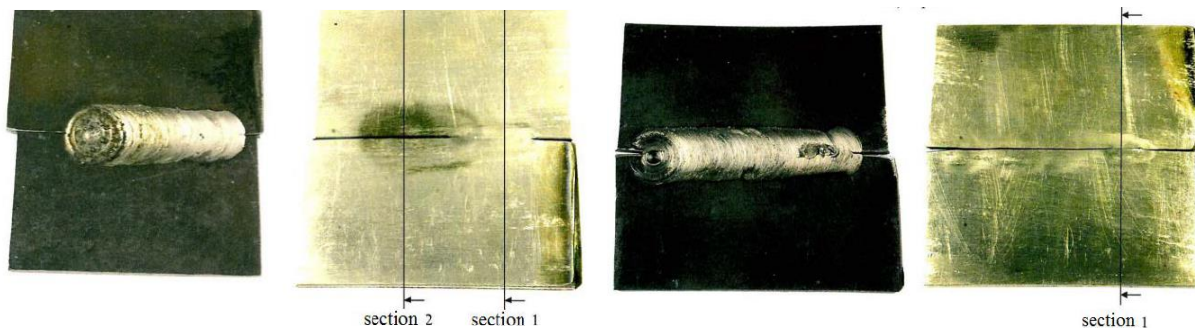


Figure 2.24 On the left specimen N.2, on the right specimen N.1[29].

The welded joint was observed only on the outer surface of the specimens; on the opposite surface, there is a welded area of 6 mm in length, and in the remaining area, the boundary between the plates is visible on the surface. Based on the previous experiments I.K.Chernykh et al. decided to change the tool and then use a carbide tool obtaining much better results from the point of view of joint quality and tool wear. Following, **Fig. 2.25**, are pictures of the tool after welding and of the joint made[29].

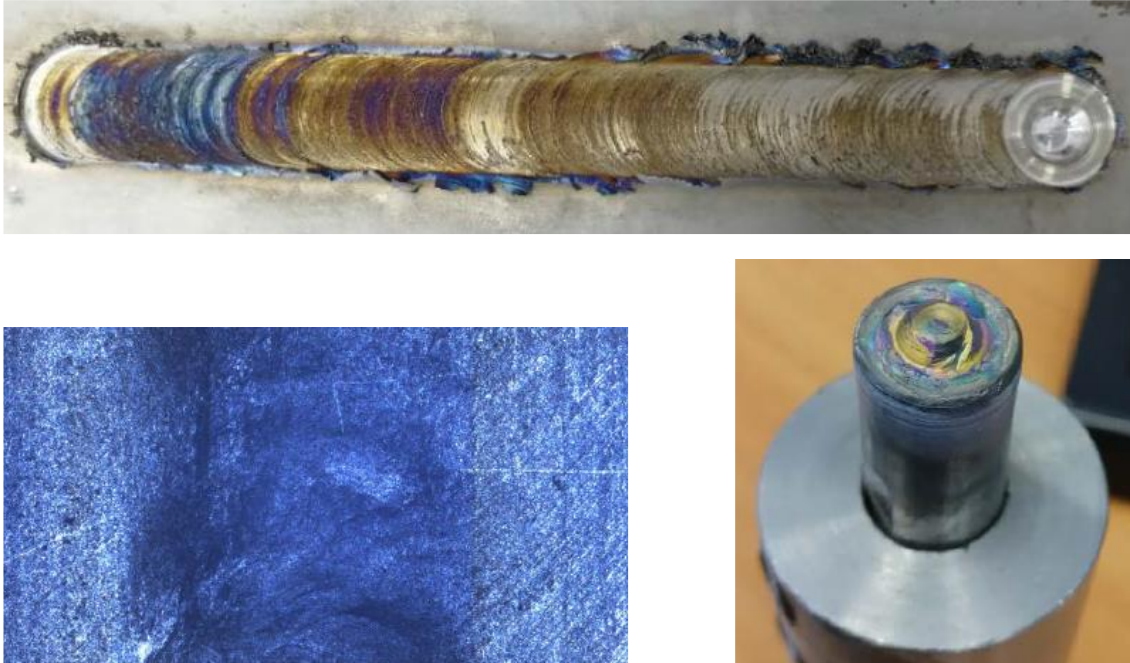


Figure 2.25 Above Specimen N.8; below, on the left the back side of the weld and on the right the worn FSW carbide tool[29].

To avoid the problems previously noted, the tools are manufactured using *Refractory Metals*. The refractory metals (molybdenum, tungsten, tantalum, and niobium) are used for their high-temperature characteristics and high density. Considered among the strongest alloys between 1000 and 1500 °C (1830 and 2730 °F), refractory metals are produced in single phase and consequently the mechanical resistance is maintained until the melting-point temperature. However, at high temperatures, niobium and tantalum easily react with oxygen, reducing the ductility of the alloy. Major disadvantages of using refractory metals include high cost, long lead times, limited availability, and difficulty in processing. They are usually processed by sintering processes. Among the main refractory metal alloys used for the tools in titanium FSW processes, the most widely used is the tungsten-based alloy. Four alloys are mentioned and described below:

- WC.
- W-25%Re.
- Densimet.
- W-1%LaO<sub>2</sub>.

Tungsten rhenium alloy has a high cost due to the value of the raw materials but has as main advantage the high working temperature. In terms of disadvantages, it has machining characteristics that require grinding processes (more difficult and expensive than conventional machining). Densimet consists of an iron-nickel or iron-copper matrix within which small tungsten balls are bonded. The main advantage is the ease of machining with conventional methods and a low raw material cost. Finally, there is the W-1%LaO<sub>2</sub> alloy which has the machinability and cost of Densimet but the high temperature resistance of tungsten-rhenium based tools. The ultimate tensile strength temperature dependence of tungsten, W-27%Re, Densimet, and W-1%LaO<sub>2</sub> is shown in **Fig. 2.26**[10].

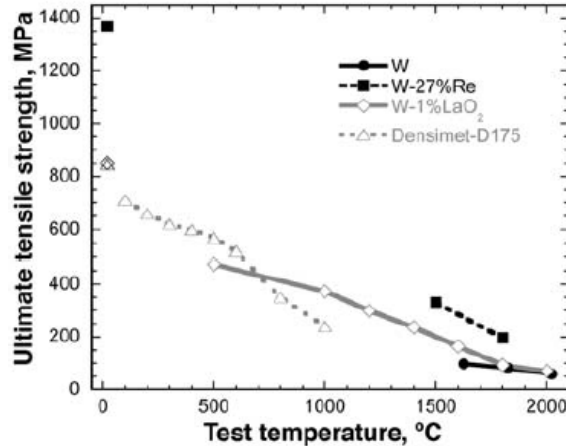


Figure 2.26 Elevated-temperature tensile properties for W, W-27%Re, Densimet D175, and W-1%LaO<sub>2</sub>[10].

In the work performed by Fall A. et al., the wear characteristics of the WC tool, used to weld two-millimetres sheets of Ti-6Al-4V, are analysed. In addition, damage, and microstructural changes in relation to tool wear are also analysed and discussed, the impact of each process parameter on the wear rate and the most influential ones identified. The results obtained are the following:

1. The tool wear is strongly influenced by the rotation speed of the tool, **Fig. 2.27**, especially the lower the speed the higher the wear.
2. Radial wear of the pin is strongly influenced by the rotation speed of the tool, the lowest wear rate was recorded for low rotation speeds[21].

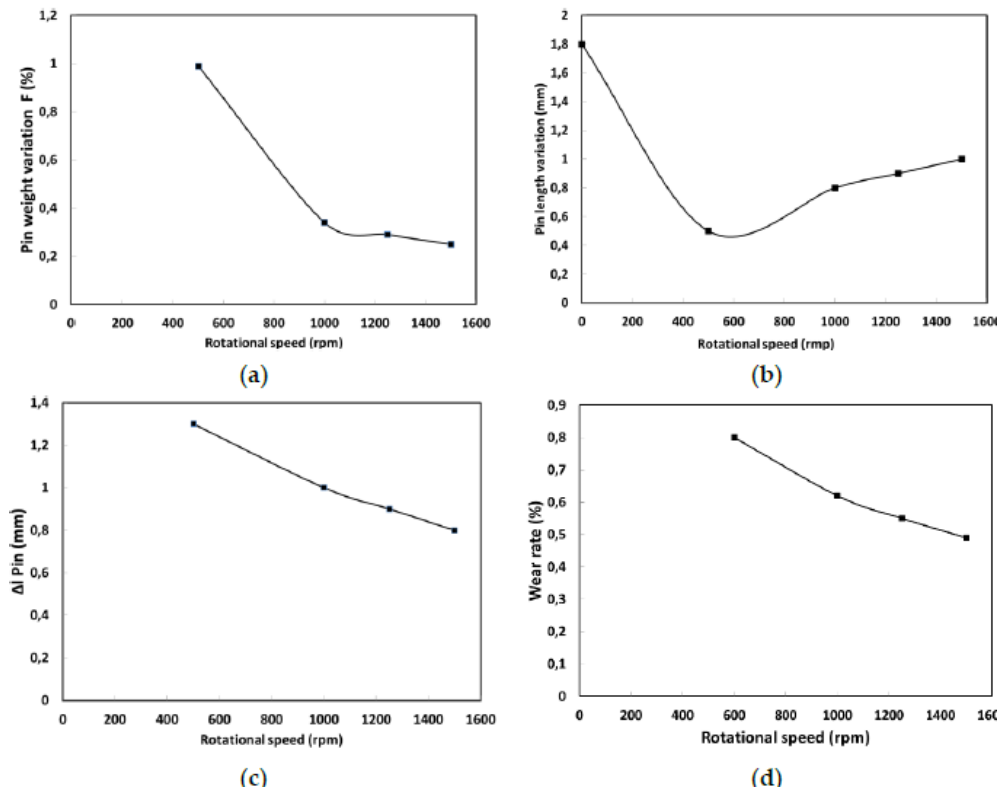


Figure 2.27 Wear measurement after 10 cm welding: (a) weight loss data as function of rotational speed; (b) pin length evolution as function of processing parameter; (c) pin length variation with rotational speed; (d) wear rate as function of rotational speed[21].

In the research work carried out by Wang J. et al., FSW tests were performed on Ti-6Al-4V plates with a thickness of 2.5 mm. In addition, the performance of three types of tools one W-1.1%La<sub>2</sub>O<sub>3</sub> and two WC-Co based tools were analysed. For convenience, the three tool materials will be referred to as W-La, CY16 (nominal composition of 73% WC, 8% TiC and 11% TaC) and WC411 (nominal composition of 89% WC and 11% Co) correspondingly. The results obtained are the following, **Fig. 2.28**:

1. Tool degradation was observed in W-La due to plastic deformation that can be reduced by increasing the pin diameter. High shear-induced cracks were observed at the pin tip and tool debris was left in the workpiece.
2. The performance of the tungsten carbide tools was determined by their chemical composition. In the CY16 tool, fracture failure was observed, whereas in the WC411 tool with better fracture toughness, only microfracture was observed in when fracture propagation was inhibited[30].

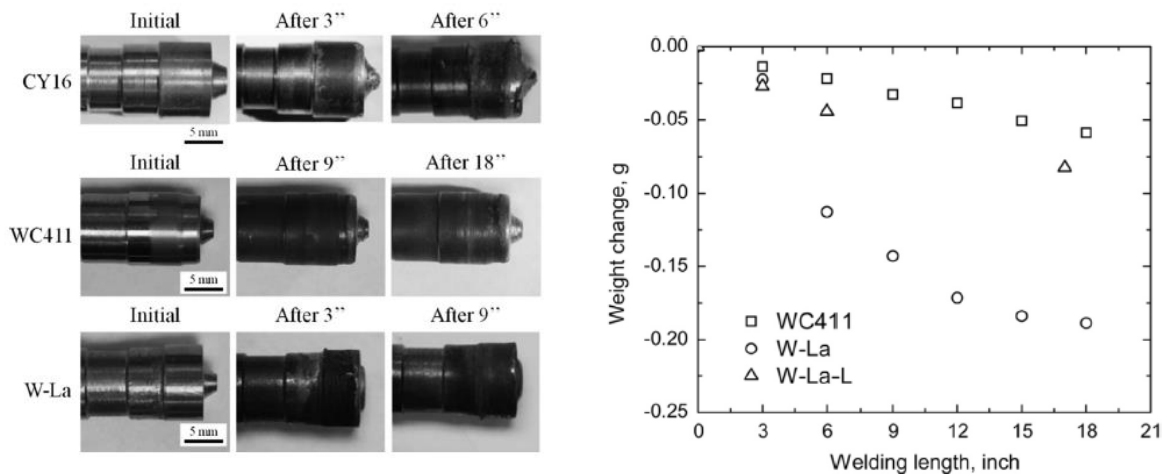


Figure 2.28 On the left appearance of the tools after different welding lengths. Note that the total length of accumulative welds is different for the three different tools. On the right weight change versus total welding length[30].

Interesting are the studies carried out by G. Buffa et al. where it is shown the different state of wear of three tools made of different materials used for the realization of joints between two titanium sheets in butt configuration. Titanium alloy sheets in the following composition Ti-6AL-4V with dimensions of 100 mm x 200 mm x 3 mm were used to make the joints. Welding was carried out under different process conditions; in particular, the selected tool rotation speeds were 300, 700 and 1000 rpm, and the feed speed was set at 35 mm/min. The sinking speed is kept constant at 0.6 mm/min, this parameter is of crucial importance for the life of the tool because the sinking phase is the most dangerous as the tool meets the still cold titanium. The geometry of the tools used remains unchanged for each header material, it is characterized by a 16 mm shoulder and a 30 degrees conical pin 2.6 mm high with the largest diameter of 5 mm. Three different tool materials are tested in the experiments: K10, k10-K30 and W25Re. The first two are tungsten carbide-based materials with a certain percentage of cobalt, characterized by a very fine grain microstructure. As for W25Re, the presence of 25% of pure rhenium gives an increase in recrystallization temperature, ductility and tensile strength compared to commercially pure tungsten. Following, in **Fig. 2.29**, the chemical composition and mechanical properties of the previously described materials.

Material	WC %	Co %	Density [g/cm <sup>3</sup> ]	Hardness HV10	Transverse rupture strength (TRS) [MPa]
K10	95.8	4.2	15.05	2300	3700
K10-K30	88.0	12.0	14.10	1760	4600

Material	W %	Re %	Density [g/cm <sup>3</sup> ]	E [Gpa]	Tensile strength (20°C) [MPa]	Tensile strength (1500°C) [MPa]
W25Re	75.0	25	19.7	410	3800	330

Figure 2.29 Chemical composition (wt%) and mechanical proprieties of the tools[31].

Important observations can be deduced from the figure below. Regarding the K10 material, there is no data corresponding to a rotation speed of 300 rpm; this indicates that tool failure occurred during the first weld, in all three tests performed at 300 rpm of K10. This is due to the combination of two factors: the “cold” welding conditions and the brittle behaviour of this alloy. In fact, the lowest rpm corresponds to the lowest Specific Thermal Contribution (STC) given to the joint and, consequently, to an insufficient softening effect of the titanium plates. By increasing the STC and continuing to work with the same tool material, some plates could be successfully jointed. However, the overall tool life is very low, showing unacceptable values for industrial applicability. For the other two materials, there is a significant increase in tool life, **Fig. 2.30**.

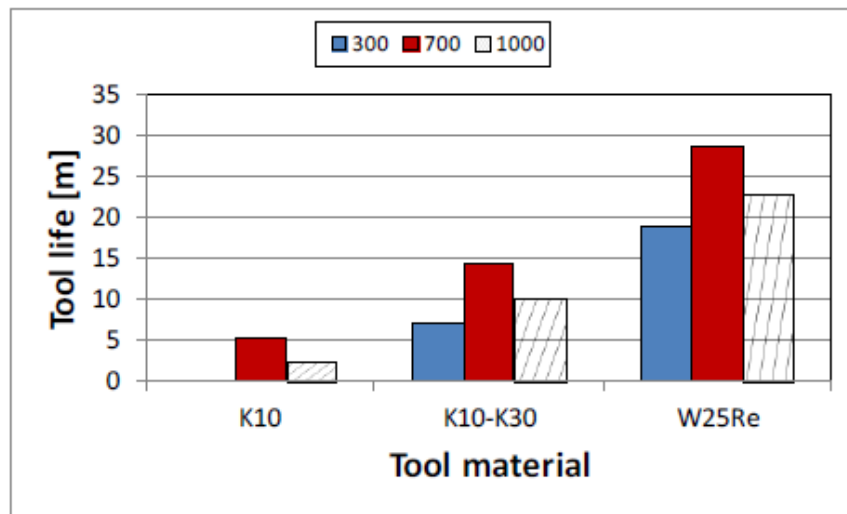


Figure 2.30 Tool life at the varying of tool material and process conditions (tool rotating speed)[31].

Images of the three damaged tools are presented in **Fig. 2.31 (a to c)**. As it can be observed, the two WC-based alloys show a completely different behaviour: K10 shows a typical brittle fracture due to the combination of excess torque, bending stress and compressive force. The extreme mechanical stress conditions to which the tool is subjected, together with the imperfect rigidity of the machine and the small vibrations generated by the random inhomogeneity of the material, led to an early failure. As for the K10-K30 alloy, a ductile type of failure mode is evident. Significant deformation occurs progressively in the shoulder, where, at the end of the tool’s life, an obvious mushrooming effect occurs. In addition, the tool ends its life cycle when the pin, previously mushroomed, is completely torn from the surface of the shoulder. Finally, visible signs of adhesive wear of the coated titanium on the shoulder surface of the tool can be seen. Because of the observations made previously, it appears that the quality of the welds progressively decreases as the tool travels meters of weld length. Finally, when observing the W25Re tool after failure, no obvious signs of deformation or adhesive wear were found. On the contrary, a mid-height fracture

of the pin is noted, resulting in inadequate penetration into the titanium plates generating joints with the presence of the tunnel defect. However, it can be observed that the damaged pin does not show visible signs of deformation and mushrooming.

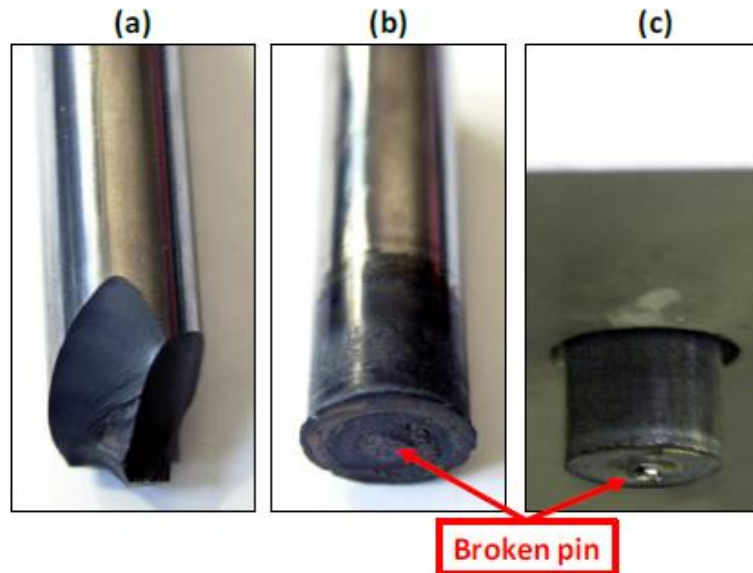


Figure 2.31 Broken tools at end of their life: (a) K10, (b) K10-K30 and (c) W25Re[31].

Following, in **Fig. 2.32**, is a photo of the tool in W25Re at the midpoint of its life cycle (about 12 meters)[31].

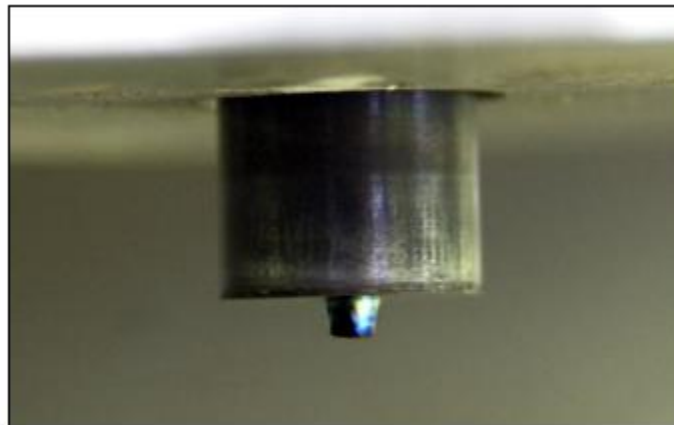


Figure 2.32 W25Re tool at about half of its life cycle. 700 rpm case study[31].

Ultimately, we examine the studies carried out by K.Reshad Seighalani et al. where the optimal process parameters and tool design are researched to achieve welding by FSW of two pure titanium sheets. The commercially pure titanium sheets used for testing are 3 mm thick and the dimensions in the plane are 140 x 55 mm. The chemical composition and mechanical properties of this material are given in the Fig. 2.33 below.

Other	Mn	Fe	Al	Ti
Under 0.05	0.05	0.04	0.15	99.7
Property	hardness HV, 30 kgf	Elongation, %	US, MPa	YS, MPa
value	148	39	402	342

Figure 2.33 Chemical composition and mechanical propriety of the tool[32].

The tests involve the use of tools that are different in terms of the material with which they are made but with the same geometry, a pin 2.85 mm high and with a diameter of 5 mm and the shoulder with a diameter of 18 mm. The operating conditions of the individual tests are summarized in the Fig. 2.34 below.

Test condition	Integration between pin and shoulder	Pin profile	Pin material	Shoulder material	Cooling system	Tilt angle	( $\omega$ (rpm), $v$ (cm/min))	Shielding gas
1	Integrated in one piece	Threaded cylinder	HSS	HSS	...	3°	(1250,3.2)	...
2	Integrated in two piece	Threaded cylinder	WC	HSS	Compressed air	3°	(1250,3.2)	...
3	Integrated in two piece	Simple cylinder	WC	W	...	1°	(1250,3.2)	...
4I	Integrated in two piece	Simple cylinder	WC	W	Compressed air	3°	(1250,3.2)	...
4II	Integrated in two piece	Simple cylinder	WC	W	Compressed air	1°	(1250,3.2)	...
4III	Integrated in two piece	Simple cylinder	WC	W	Compressed air	1°	(1500,6)	Argon

Figure 2.34 Test conditions based on tool material and design and cooling system[32].

Fig. 2.35 shows that in condition 1 the penetration of the tool and transversal feed of the workpiece lead to complete failure of the pin and significant wear of the shoulder caused by the heat generated by the friction between the tool and the base metal, which means that the weld in the final part is decidedly weaker.

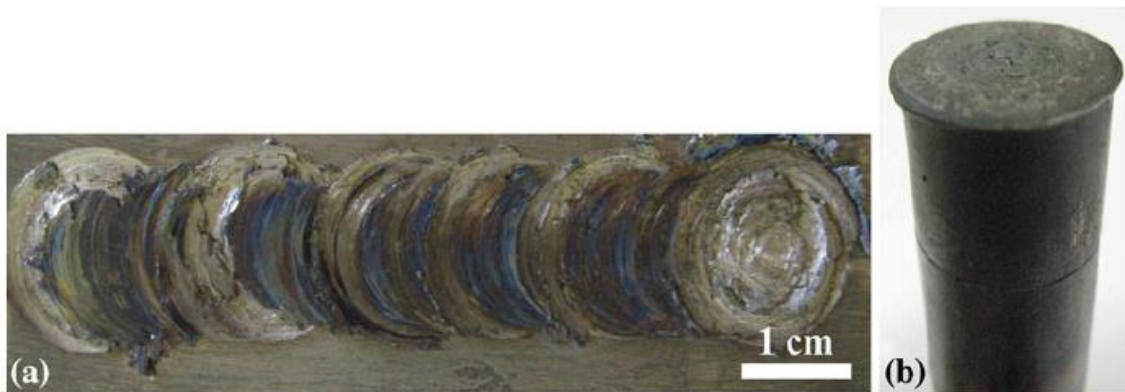


Figure 2.35 (a) Photograph made from the joint formed made under condition 1; (b) used tool made under condition 1 at the end of the FSW[32].

In condition 2 the tool, consisting of a WC pin and an HSS shoulder, has a threaded cylinder pin geometry with a 0.8 mm pitch. In addition, the tool is cooled with a jet of compressed air.

**Fig. 2.36** shows the shape of the tool after finishing the welding process and the joint formed in condition 2. Although the tool was cooled with a jet of compressed air, significant tool wear at the end of the welding process can be clearly observed, despite this, the pin height did not change during welding. The severe wear of the HSS shoulder generated very poor weld surface quality.

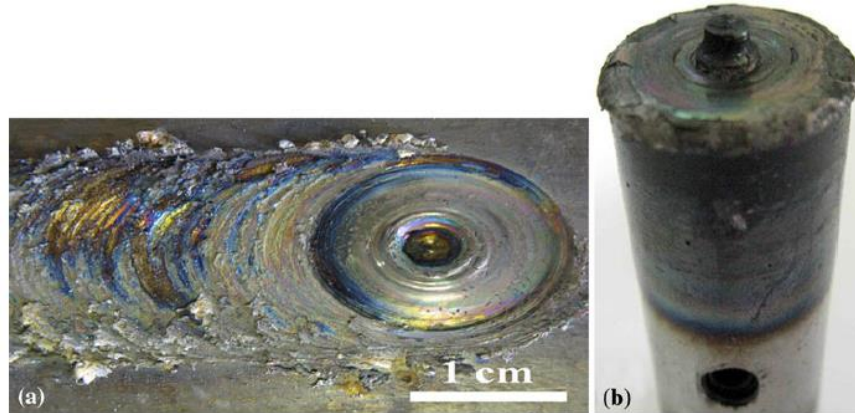


Figure 2.36 (a) Photograph of the joint surface formed under the condition 2, (b) tool under the condition 2 with WC pin and HSS shoulder at the end of FSW process[32].

In Condition 3, with a tool consisting of a WC pin and a W shoulder, the tool tilt angle is set to 1°, and the air cooling of the tool is removed. As can be seen in **Fig. 2.37**, in the cross section of the weld there is the formation of some cracks. These cracks, caused by the tool shoulder, indicate intense wear and penetration of the tool material into the joint area.

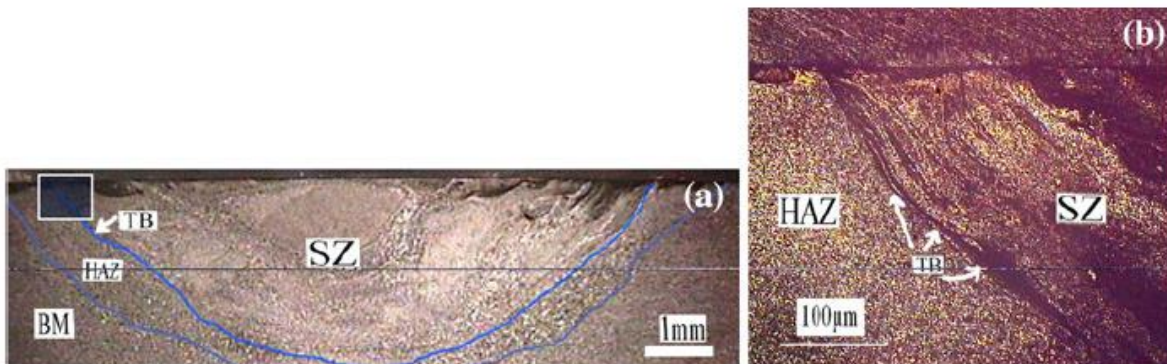


Figure 2.37 Photograph made from cross section surface of the joint formed under the condition 3[32].

Macroscopic views of the joint cross-section made in condition 4III, **Fig. 2.38**, show an absence of any type of weld defect in the region where it occurred. **Fig. 2.39** shows the top and rear views of the joint and the tool used at the end of service.



Figure 2.38 Macroscopic view of the joint cross section in condition 4III[32].

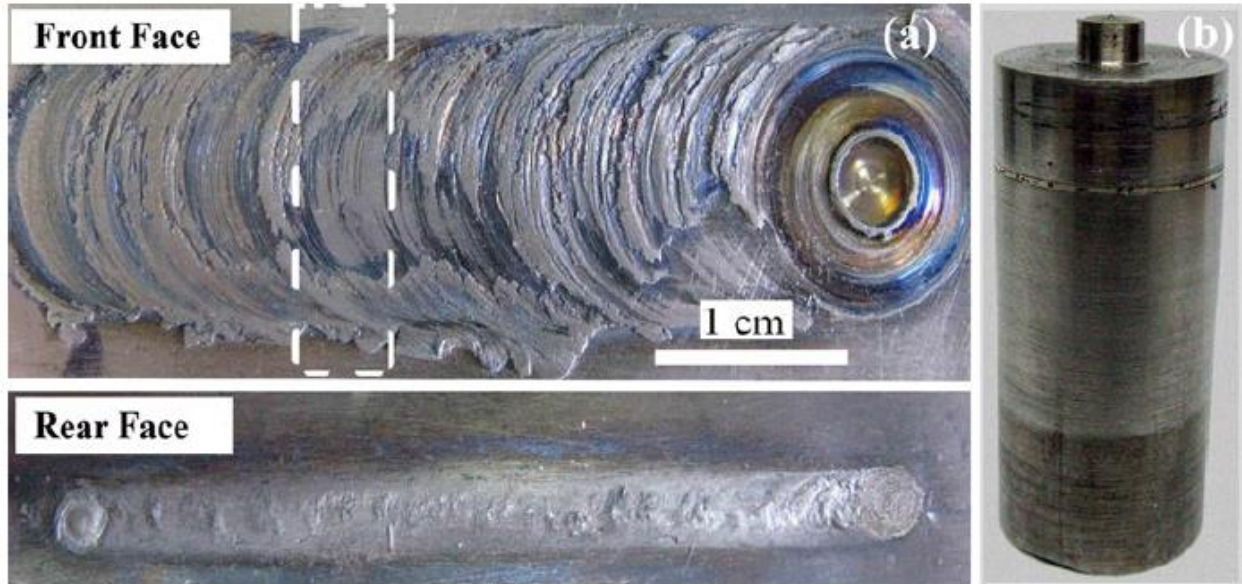


Figure 2.39 (a) Joint formed by condition 4III with the tilt angle of 1°, (b) used tool in condition 4III after FSW[32].

It can be seen from the study of the macrostructure of the various welds that the first and most fundamental step in obtaining a defect-free weld joint is the correct choice of material and tool geometry and then, only later, the optimization of the process parameters[32].

## 2.4. APPLICATIONS FIELDS OF FSW OF TITANIUM

TWI together with Airbus Defence have worked for the European Space Agency (ESA) in the search for cost-effective production methods for the manufacture of titanium propellant tanks. The project studied the feasibility of using the fixed-shoulder Friction Stir Welding technique (SSFSW) for cylindrical welding of titanium alloys suitable for the fabrication of launch vehicle propellant tanks. Current manufacturing methods are extremely expensive and involve very long processing times as well as excessive production material waste due to complex forging, forming and electron beam welding or TIG welding techniques. A representative demonstrator tank design, **Fig. 2.40-2.41**, has been developed and agreed with ESA and Airbus.



Figure 2.40 Propellant tank example[33].

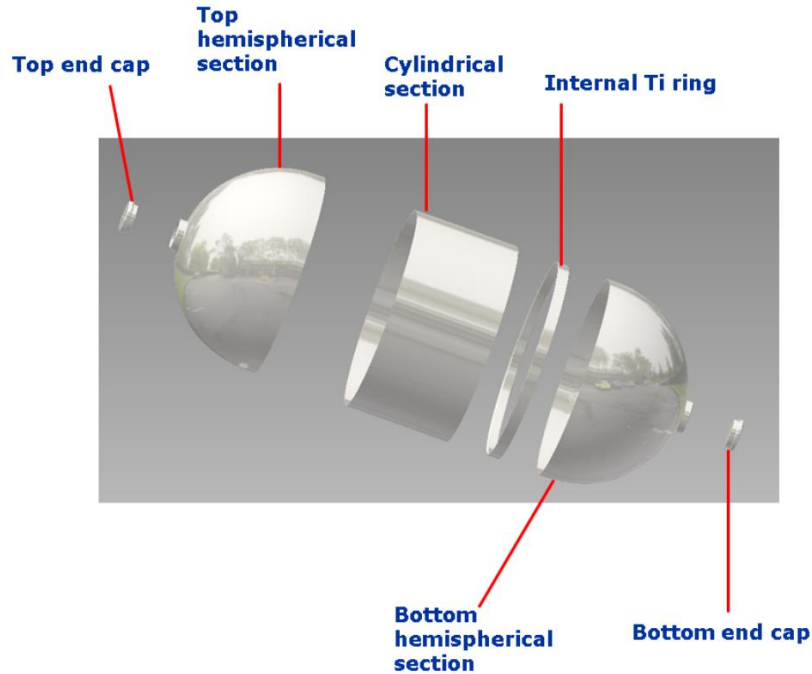


Figure 2.41 Exploded view of the titanium alloy tank[34].

Welding trials using stationary shoulder friction stir welding (SSFSW) tools have demonstrated good results, producing high-quality welds and, importantly, demonstrating a great extension in the lifetime of the tool. TWI in August 2016 successfully performed the world's first circumferential welding of two 420 mm cast titanium cylinders using SSFSW, **Fig. 2.42**.

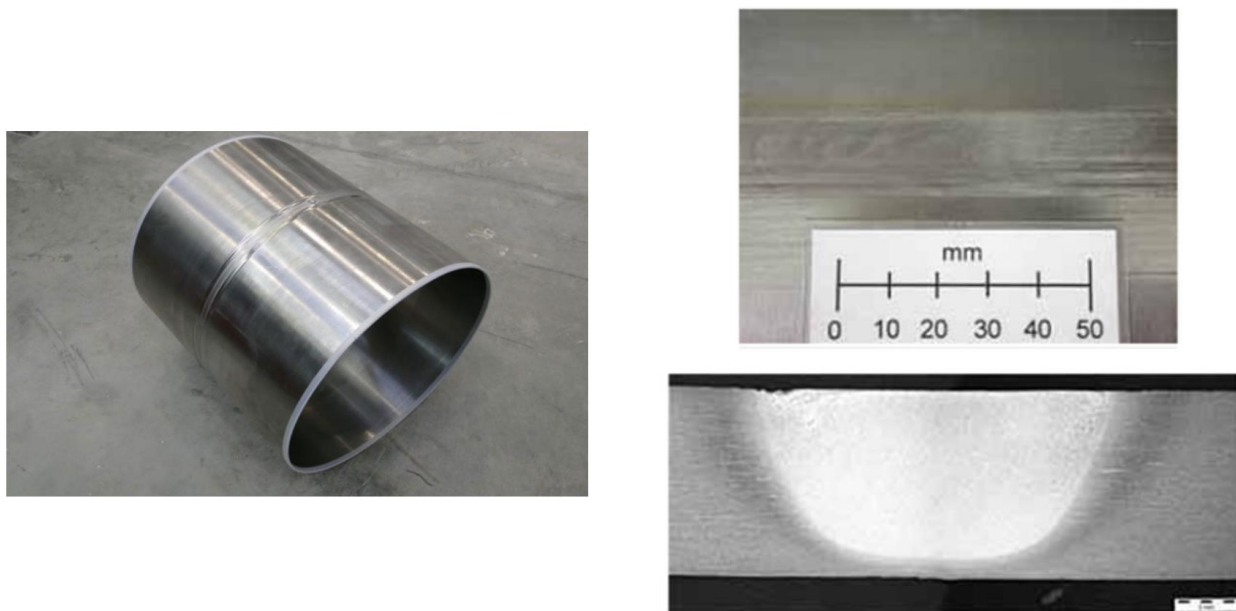


Figure 2.42 On the left the first full circumferential FSW, on the right the surface of a Ti-6Al-4V weld (top) and macrostructure of a weld (bottom) made with SSFSW tool[33], [34].

Subsequently, the test pieces were then subjected to non-destructive test (NDT) and mechanical evaluations to confirm the mechanical qualities of the joint, **Fig. 2.43 - 2.44 - 2.45**[33]–[35].



Figure 2.43 On the left the support of the circumferential FSW, on the right welding underway on the cylinder-cylinder[34].

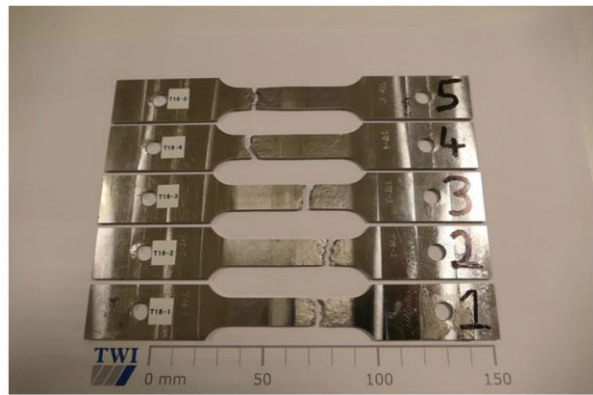


Figure 2.44 On the left cylinder-cylinder weld cut up for mechanical testing, on the right cast Ti-6Al-4V Alloy FSW - Tensile tests[34].



Figure 2.45 On the left friction stir welded hemisphere-cylinder for residual stress analysis, on the right friction stir-welded titanium propellant tank[34], [35].

### 3. EXPERIMENTAL PROCEDURE

Several experimental tests, to research the optimal process parameters for the fabrication of a good quality joint using FSW technology, were performed using commercially pure grade 2 titanium sheets. The tests were carried out using sheets of different thicknesses and dimensions:

- Between two 1 mm thick sheets (100x100 mm).
- Between two 2 mm thick sheets (100x150 mm).

Below, in **Fig. 3.1**, the list of chemical and mechanical proprieties.

#### Chemical properties

Property	Value
Carbon	0,08 %
Hydrogen	0,02 %
Iron	0,3 %
Nitrogen	0,03 %
Oxygen	0,25 %
Titanium	Balance

#### Mechanical

Property	Temperature	Value	Comment
Charpy impact energy, V-notch	23.0 °C	40 - 82 J	Typical value
Elastic modulus	23.0 °C	103 GPa	Typical value
Elongation A50	23.0 °C	28 %	Typical value
Hardness, Vickers, 10	23.0 °C	160 - 220 [-]	Typical value
Reduction of area	23.0 °C	55 %	Typical value
Tensile strength	23.0 °C	485 MPa	Typical value
Yield strength Rp0.2	23.0 °C	350 - 450 MPa	Typical value

Figure 3.1 Chemical composition of Ti grade 2 (top), mechanical properties of Ti grade 2 (bottom).

The joints were made both in a lap configuration using a tungsten alloy tool (W-25%Re). Below, in **Fig. 3.2 – 3.3**, are the pictures of the machine used to make both the weld and a drawing of the tools, used to join 1 mm thick sheets and 2 mm thick sheets, with the relevant dimensions.

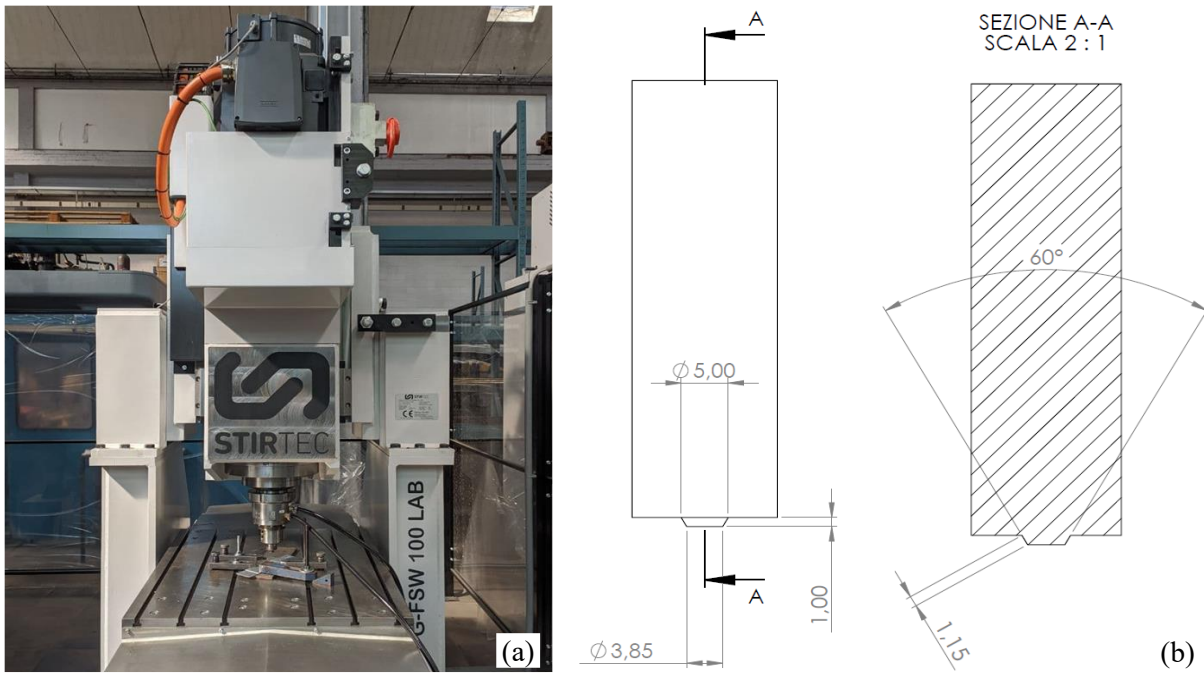


Figure 3.2 On the left is a photo of the machine used for the FSW, on the right is a drawing with the main dimensions of the tool used for the 1 mm thick sheets.

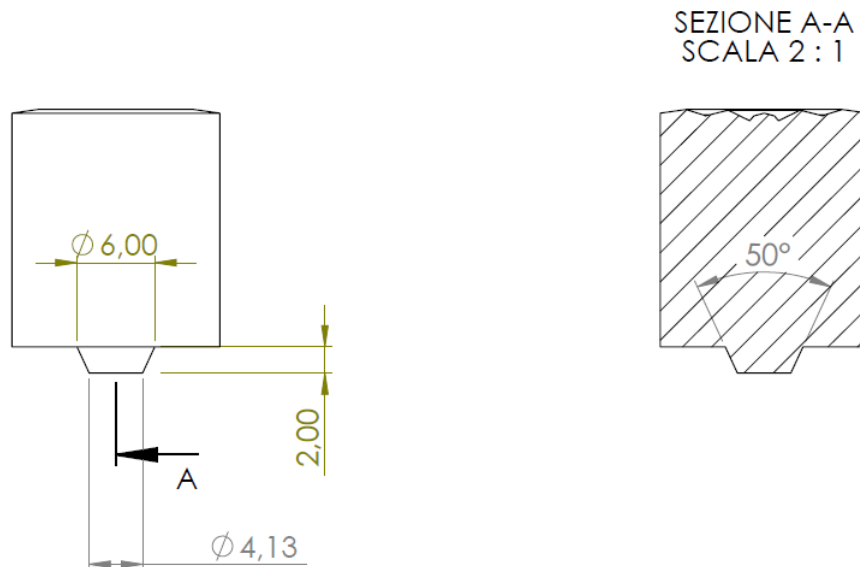


Figure 3.3 Drawing with the main dimensions of the tool used for 2 mm thick sheets.

The clamping system of the titanium sheets, **Fig. 3.4**, is important for the creation of the joint; it was created ad hoc and is fundamental to avoid any form of harmful vibration and to obtain a precise, high-quality weld. Below is a picture of the clamping system in which you can also see

the presence of a protective bar made of tungsten carbide placed under the sheets to be welded, which prevents damage to the clamping system if the tool pierces both sheets to be joined.

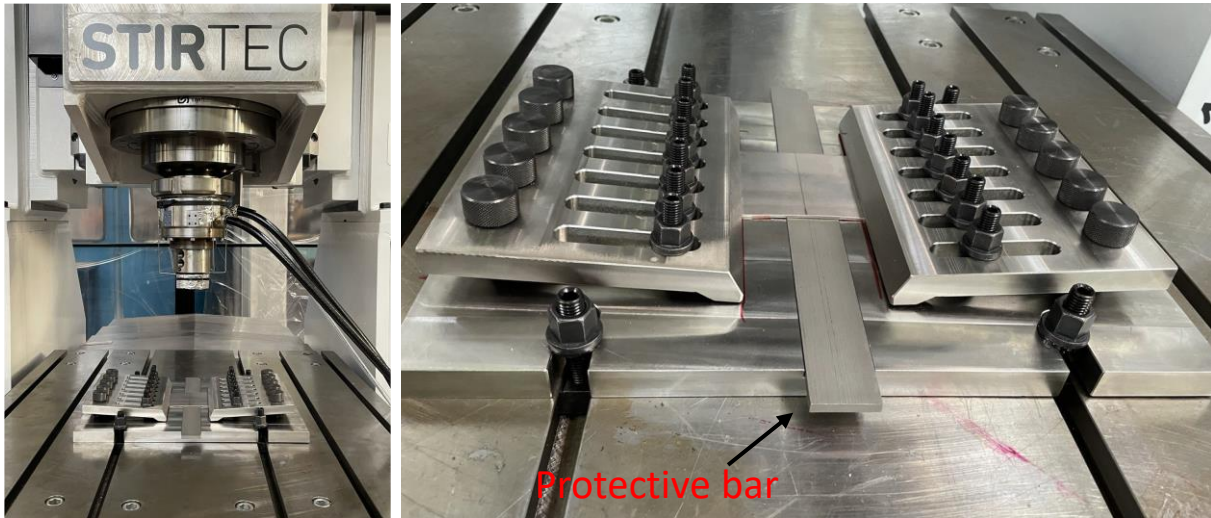


Figure 3.4 On the left a picture of the tool holder, on the right a picture of the sheet metal clamping system.

After several attempts, by varying the various process parameters including tool rotation speed and feed rate, it was possible to obtain fully welded samples to be analysed by metallographic analysis. The process parameters used to make these samples are as follows:

#### **Joint 1 (1 mm sheets)**

- Rotation speed of the tool: 450 rpm.
- Feed rate of the tool: 30 mm/min.
- Dwell time: 3 sec.
- Plunge speed: varying from 2 to 3 mm/min.
- Welding length: 40 mm

#### **Joint 2 (2 mm sheets)**

- Rotation speed of the tool: 250 rpm.
- Feed rate of the tool: 75 mm/min.
- Dwell time: 5 sec.
- Plunge speed: 2.3 mm/min.
- Welding length: 110 mm

After making the welded joints, the areas in which cuts must be made are selected to obtain the different samples to be analysed in different areas of the weld line. The specimens are cut and then embedded in a polymer resin using an embedding machine. This last step allows a better handling of the specimens and a lower wear of the edges of the specimens itself. After incorporating the specimens, the polishing operation is carried out using a polishing machine. Polishing is carried out using discs of abrasive paper of increasing grain size, starting from a grain of 180 and with gradual steps you get to a grain of 4000, finally we conclude the process using as the last step of polishing a diamond paste that allows to obtain a polishing up to 1 micro-meter in size. After the polishing operations, the next step is the metallographic chemical attack carried out with an acid attack with Kroll reagent, which lasted about 30 seconds by spreading this reagent on the newly polished surface. Finally, the optical microscope analysis is carried out obtaining the images characterizing the welding area. After capturing images of the weld zone under the light

microscope, a virtual matrix is created that will serve as a guideline for making sampling points for micro-hardness analysis. Each point in the virtual matrix should correspond to a sampling point. After that, using the micro-durometer, the indentations on the sample are realized following the indications of the virtual matrix previously realized. Regarding the load applied by the indenter, a force of 500 g applied for 15 seconds was used as indicated in the literature[36].

## 4. RESULTS AND DISCUSSIONS

### 4.1. WELDING OF 1 MM Ti SHEETS

Starting from the analysis of the first joint made by joining through FSW two sheets of 1 mm thickness, it can be seen below, in **Fig. 4.1**, how the joint appears immediately after the end of the working process.

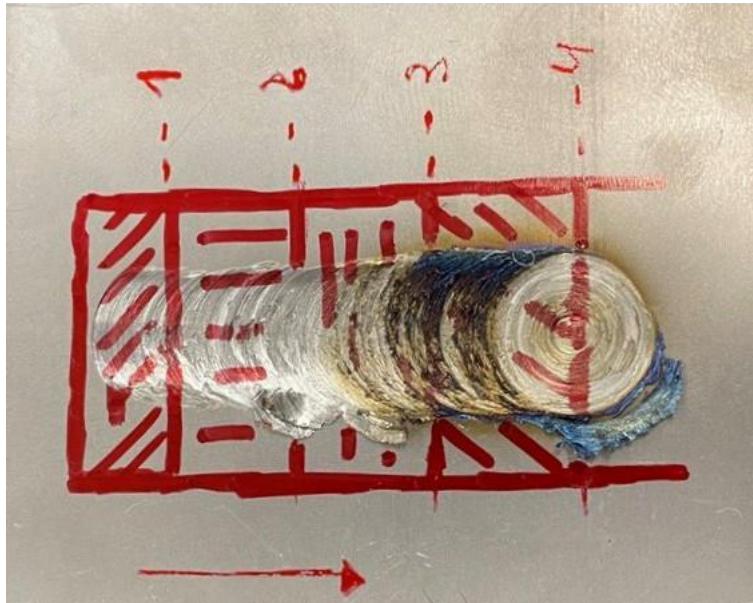


Figure 4.1 Morphology of the freshly welded joint.

From the subsequent cutting in the areas marked in red, of the sample obtained, only those in which welding has taken place correctly are selected. Below, in **Fig. 4.2**, is the sectioning of the cuts made and optical microscope images of the weld zones of the specimens examined.

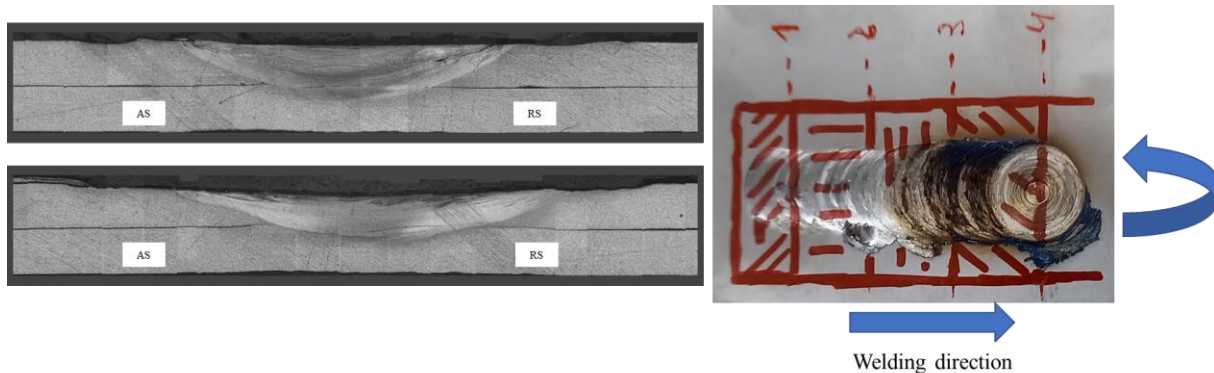


Figure 4.2 On the right the cutting indications for the specimens to be analysed, on the left the micrographs of the weld surfaces of the indicated specimens.

Below, in **Fig. 4.3**, is a comparison of the section of the junction, viewed under an optical microscope, with and without the presence of the indentations made using a micro-durometer.

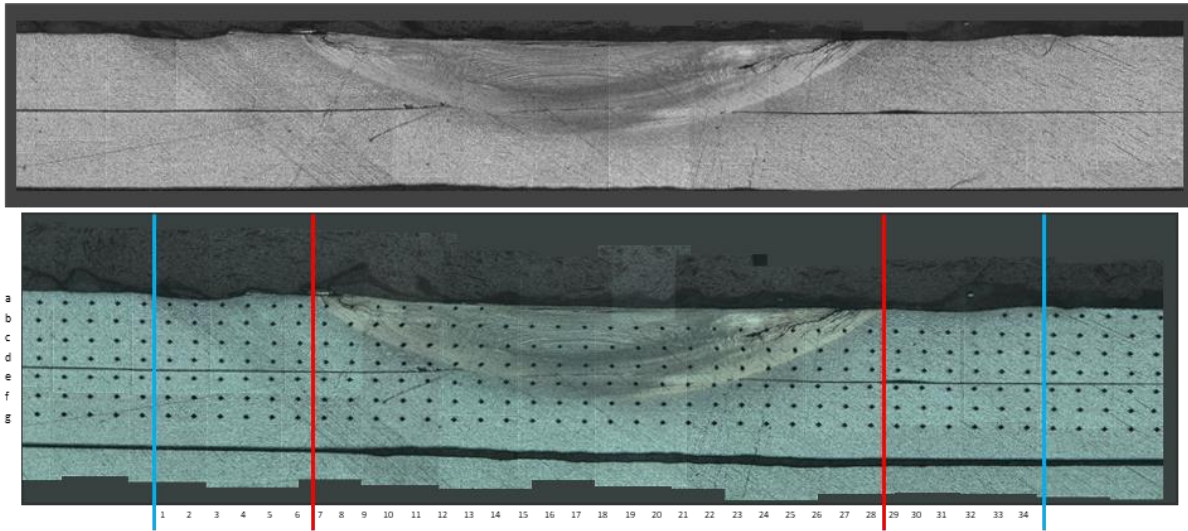


Figure 4.3 The micrograph of the weld section (top), the micrograph of the weld section after performing micro-durometer indentation (bottom).

In the image with the indentation, you can see the structure of the virtually created matrix in which the letters (a to g) correspond to the rows and the numbers (1 to 34) to the columns. The spacing between rows and between columns established previously is 250 microns and 350 microns respectively.

Once the indentations were made, the optical microscope was used again to capture images of each indentation at 100x magnification. This allows a more precise measurement of the diagonals of the impression, using a micro-meter ruler, measures that will be included in an excel file created ad hoc for the calculation of Vickers hardness in each indented point. These data were then reprocessed to obtain graphs and hardness maps of the entire weld surface, **Fig. 4.4**.

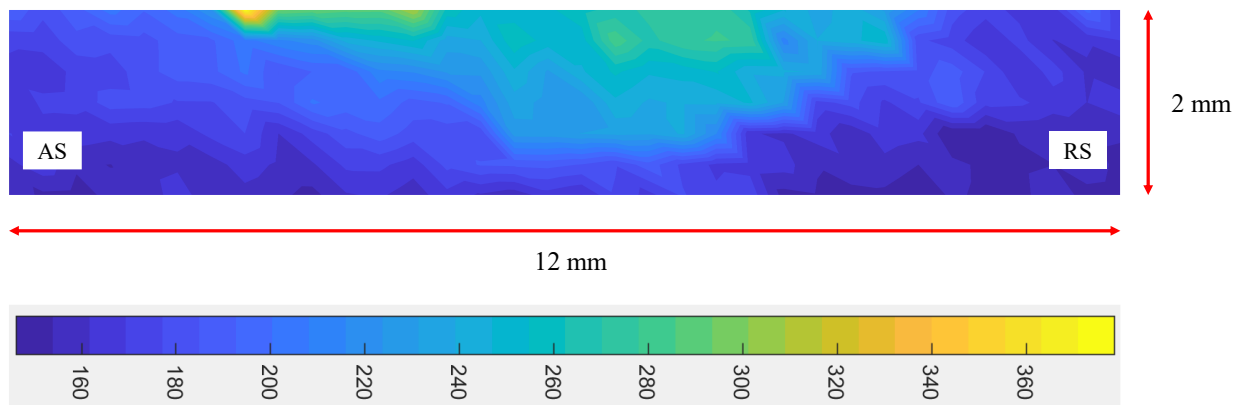


Figure 4.4 The map of hardness variation in the weld section.

Next, we can see a realization of the micro-hardness trend, **Fig. 4.5**, along the transverse direction of the joint section obtained by averaging the values located along the same vertical position.

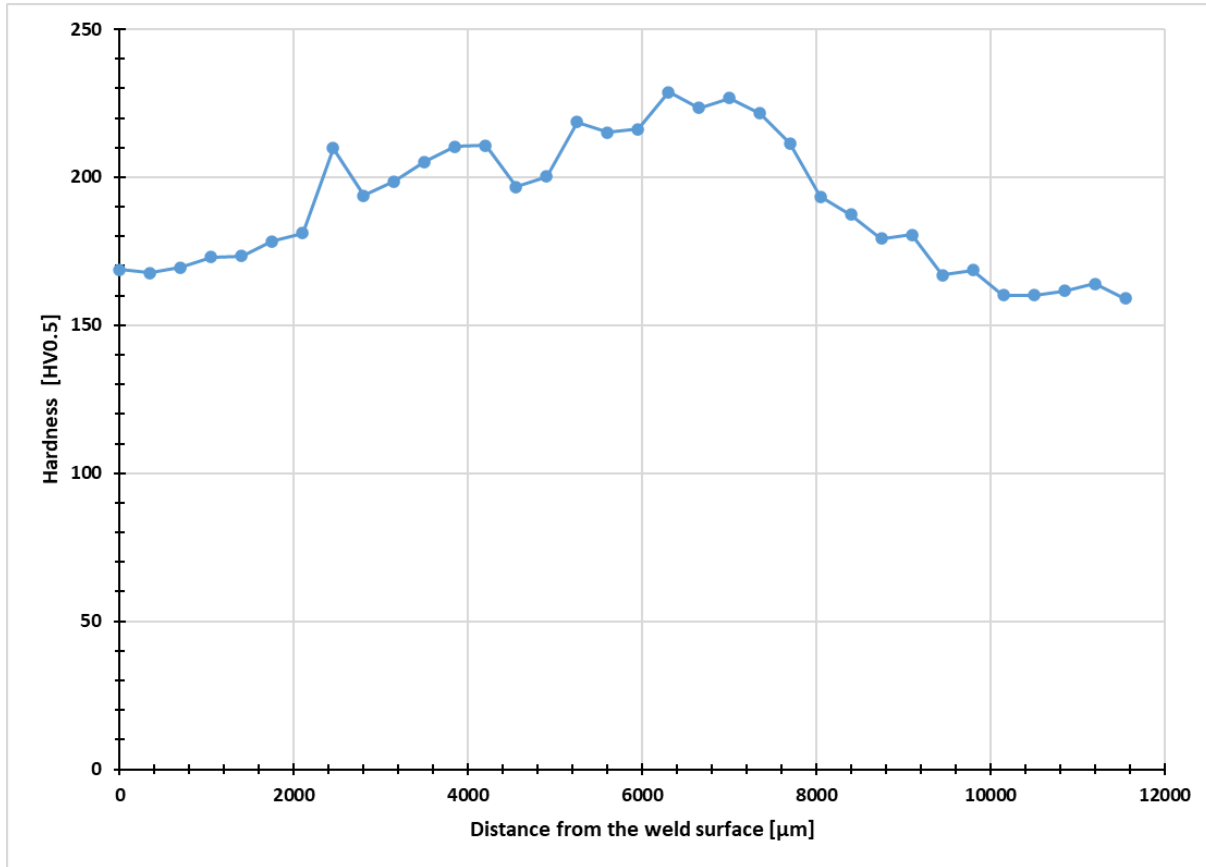


Figure 4.5 Graph of the hardness variation in the transverse direction of the weld section.

Both the map and the graph show how the hardness has a characteristic trend, typical of this type of welding. Because of the high plastic deformation, due to the high pressures involved and the high deformation rates, the central area (nugget area) of the joint section has an extremely finer microcrystalline structure than the virgin starting material, due to the recrystallization process that takes place in this area. Consequently, this area is the one with the highest hardness, with peaks up to 226 HV, with a decrease of the same both moving to the right and to the left compared to the central area. This decrease in hardness in both directions comes from the fact that the areas far from the tool pin are less affected by the action of the tool. The decrease in hardness tends asymptotically to the same value both to the right and to the left, which indicates the standard hardness of the material in question without having undergone any thermo-mechanical treatment.

Despite the first good results obtained, as regards microstructural morphology and mechanical properties, in the realization of joints with 1 mm thick sheets the process is technologically unsustainable because tool wear is extremely early (a maximum of two welds can be made). The explanation for this early wear lies in the very low thickness of the sheets used. The heat generated by the friction between tool and sample due to the very thin sample is dissipated very quickly, cooling the system, and wearing out the tool very quickly. Next, **Fig. 4.6**, is a picture of the tool after a single weld.



*Figure 4.6 Pictures of the worn tool after welding a joint.*

## 4.2. WELDING OF 2 MM Ti SHEETS

As a result of this important issue, further tests were conducted on sheets with greater thickness (2 mm). Below, **Fig. 4.7**, is a picture of how the newly made joint looks.

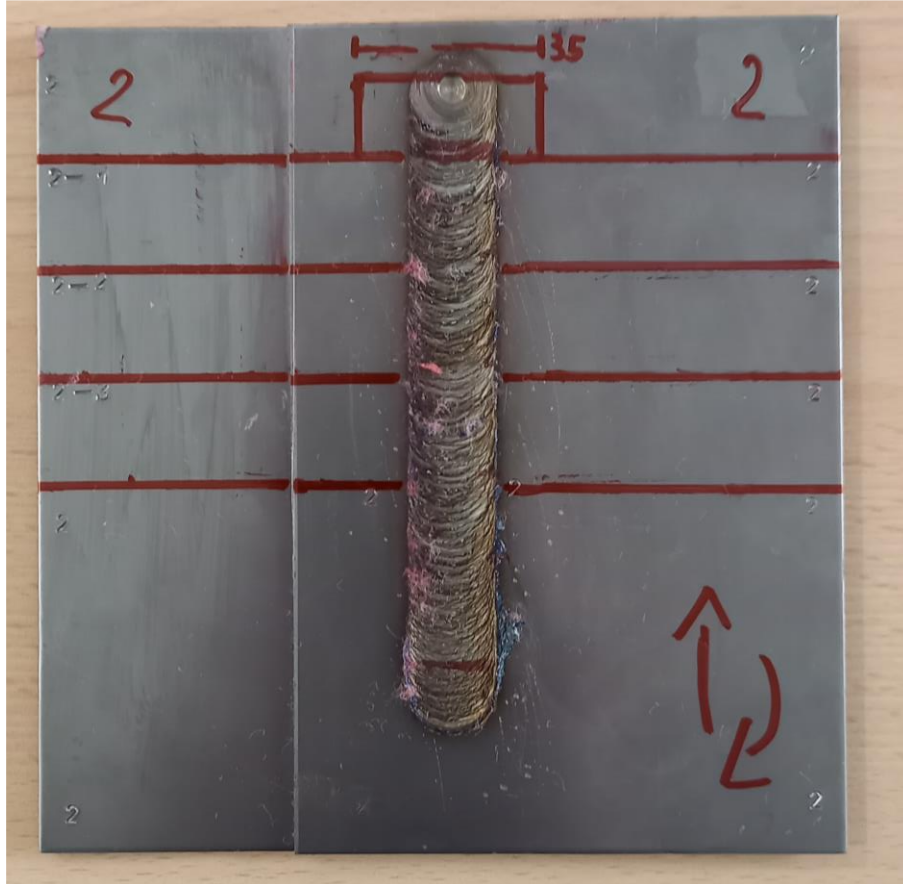


Figure 4.7 Image of the joint realized in lap configuration between sheets of 2 mm thickness.

The absence of abrasions in the vicinity of the weld is indicative of a correct heat input during the process because of a correct choice of process parameters. The metallography taken of a cross-section of the weld can be seen below in **Fig. 4.8**.

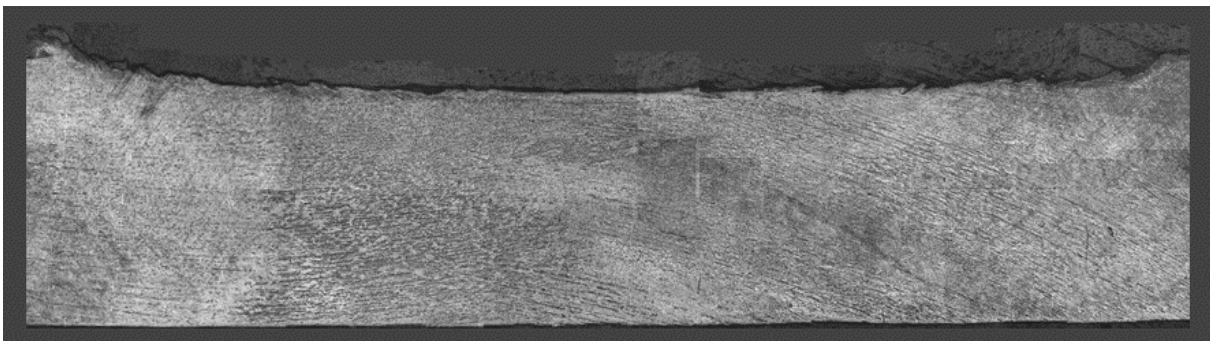


Figure 4.8 Micrograph of the weld section.

Below, in **Fig. 4.9**, is a graph showing the trend of the forces and torques brought into play during the welding process.

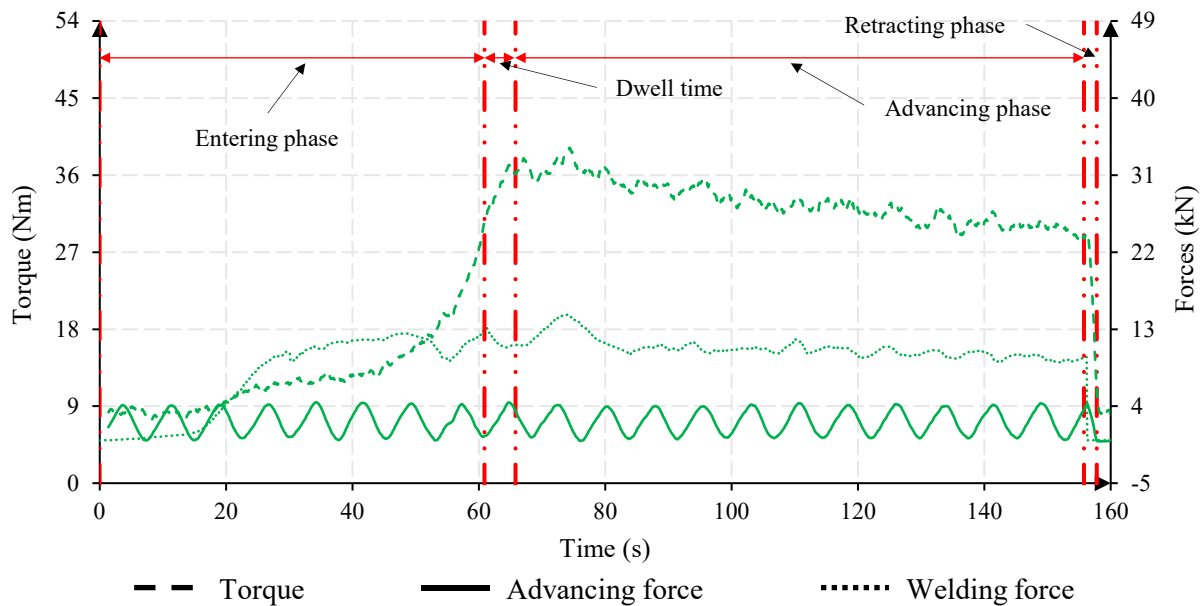


Figure 4.9 Development of the forces and torques involved during the welding process.

Very interesting is the trend of the torque applied to the tool that sees a sudden increase in correspondence of the plunge phase reaching a peak of about 37 Nm, this is due because the tool is working a cold material, in fact then during the feed phase there is a slight decrease in the torque applied, up to values of 27 Nm, due to the lower resistance of the material due to the heat generated by friction that has softened the material to be processed.

Another important parameter is the welding force, the force with which the tool is pressed against the sheets to be joined. From the graph above since the test is carried out in displacement control (welding depth), the welding force in the initial phase increases considerably, reaching values of about 15 kN. This is because the material is initially cold, so the greater the resistance it offers to the tool, the greater the welding force required to obtain the set welding depth. As welding progresses, the force remains more or less constant, but in reality, it tends to decrease slightly, because as the heat generated by the tool increases, the material becomes more malleable and offers less resistance than at the start.

Following the metallographic analysis, tensile tests were performed to test and verify whether the strength of the joint was comparable to that of the virgin material without the presence of the joint. Three samples taken from the transverse cut of the same weld but in different longitudinal positions, as shown in **Fig. 4.7**, were used for tensile testing.

The morphology of the fracture sections are as follows, Fig. 4.10 – 4.11 – 4.12.



Figure 4.10 Specimen 1 after the tensile test.

Breaking Strength: 9331.79 N  
Elongation at break: 3.775 mm

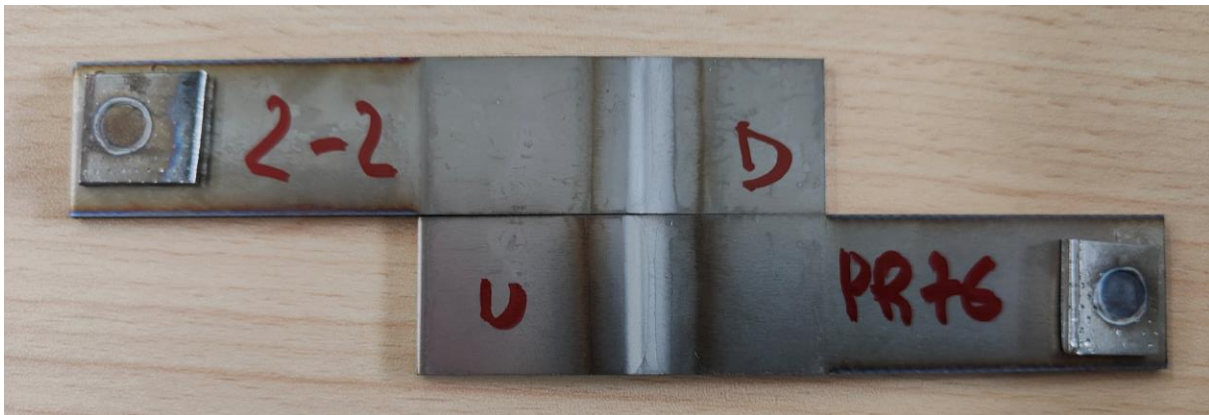


Figure 4.11 Specimen 2 after the tensile test.

Breaking Strength: 10427.56 N  
Elongation at break: 3.953 mm



Figure 4.12 Specimen 3 after the tensile test.

Breaking Strength: 9936.81 N  
Elongation at break: 4.408 mm

From the results obtained from the tensile test analysis, we can observe that compared to what is reported in the literature, in H. Liu's article[26], the results are slightly underestimated. H. Liu in fact in his research work, using the same material (Ti Grade 2), the same setting of the machine and a tool of the same size although of different material, obtains the following results, **Fig. 4.13**.

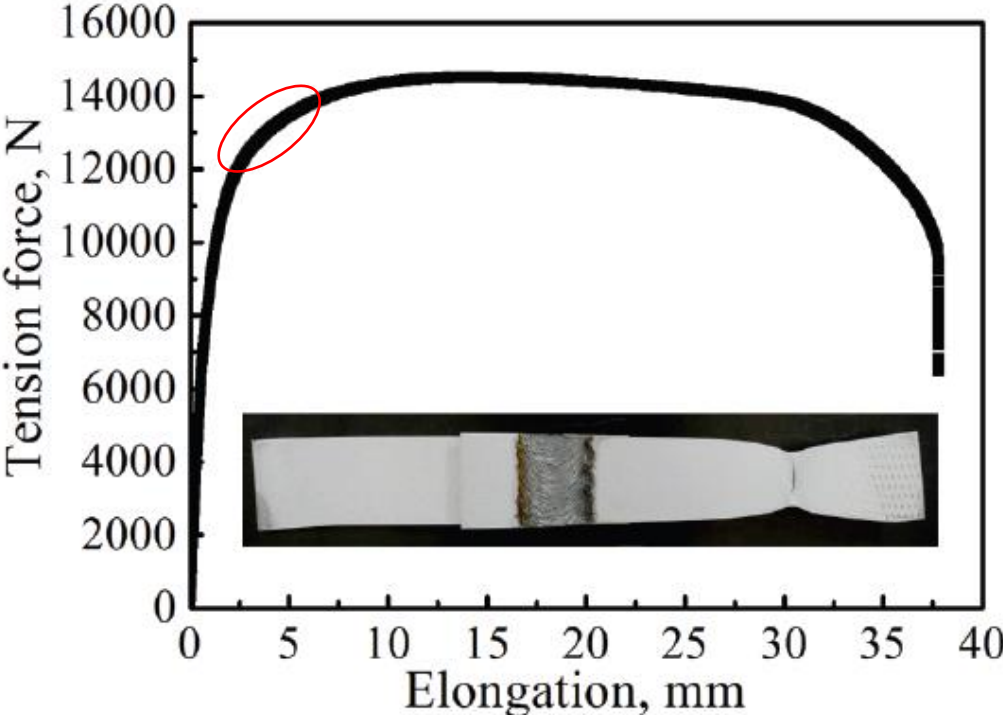


Figure 4.13 Tensile curves of CP Ti lap joint processed at 250 rpm, 75 mm/min using probe with lengths of 2.0 mm[26].

It is observed that material yielding occurs in a range of forces of 12000 N and 14000 N, observing elongations in the range of 5 mm. On the other hand, our tests, as noted above, show yield strengths of about 10000 N and elongations of about 4 mm.

## 5. CONCLUSIONS

From the results obtained from the experimental tests performed, the following conclusions can be drawn:

- 1) FSW welding of 1 mm thin sheets can give satisfactory results. However, the reduced thickness poses serious problems on tool life. Therefore, FSW may not be advantageous for such reduced thicknesses.
- 2) FSW could be a substitute for other joining technologies for welding 2mm sheets (one application could be for tanks and components for the chemical industry).
- 3) The trend of the main process parameters (torque and tool force) during the joining process has been evaluated. The analysis of these parameters could in the future be correlated with the quality of the joints. Hence the importance of being able to monitor the joining process in real time.
- 4) Based on the results observed in the literature, the data obtained in the tensile tests are underestimated presumably due to a shallow weld depth. Following the directions given to us by H. Liu in his article[26], one could increase the solder depth by increasing the pin length. However, one should be very careful in choosing the process parameters because, as noted in the same article, as the length of the pin increases, the range of optimal parameters is greatly reduced, thus risking obtaining a greater welding depth but with the presence of welding defects that would compromise the quality of the weld.

Although Friction Stir Welding technology is a well-established welding process for joining components made of steel and aluminium and their alloys, for titanium applications there are still some difficulties to be faced due to the chemical and mechanical characteristics of the material itself, such as high tool wear due to the high strength of titanium. Nevertheless, Friction Stir Welding is one of the best alternatives to traditional electric arc welding processes for joining titanium sheets, thanks to its numerous benefits, avoiding all those problems linked to the post-welding solidification process such as the formation of cracks and the establishment of internal residual stresses.

## REFERENCES

- [1] H. Liu, K. Nakata, N. Yamamoto, and J. Liao, "Friction stir welding of pure titanium lap joint," *Science and Technology of Welding and Joining*, vol. 15, no. 5, pp. 428–432, 2010, doi: 10.1179/136217110X12731414740031.
- [2] Rajiv S. Mishra and Murray W. Mahoney, "Introduction," in *Friction Stir Welding and Processing*, Rajiv S. Mishra and Murray W. Mahoney, Eds. 2007, pp. 1–5.
- [3] H. K. D. H. Bhadeshia, "Friction Stir Welding Major review on FSW Crititcal assessment: FSW of steels FSW of dissimilar materials Simple calculations for FSW." [Online]. Available: <https://www.phase-trans.msm.cam.ac.uk/2003/FSW/aaa.html>
- [4] Jacob Juma Yegon, "13 Main Advantages and Disadvantaes of Friction Stir Welding | Application of Friction Stir Welding," *HPD*, Aug. 19, 2021. [https://www.hpdconsult.com/advantages-and-disadvantages-of-friction-stir-welding/#Benefits\\_of\\_Friction\\_Stir\\_Welding](https://www.hpdconsult.com/advantages-and-disadvantages-of-friction-stir-welding/#Benefits_of_Friction_Stir_Welding) (accessed Jan. 03, 2022).
- [5] Administrator, "Friction Stir Welding (FSW) : Principle, Working, Application, Advantages and Disadvantages," *mech4study*. <https://www.mech4study.com/2017/04/friction-stir-welding-principle-working-application-advantages-and-disadvantages.html> (accessed Jan. 03, 2022).
- [6] Irfan Hassan, "Friction Stir Welding – Types, Advantages and Disadvantages," *TheEngineeringEdu*. <https://theengineeringedu.com/friction-stir-welding/> (accessed Jan. 03, 2022).
- [7] Brian Thompson, "Friction Stir Welding of Titanium Alloys," *EWI We Manufacture Innovation*. Apr. 10, 2011.
- [8] R. S. Mishra and Z. Y. Ma, "Friction stir welding and processing," *Materials Science and Engineering R: Reports*, vol. 50, no. 1–2, 2005, doi: 10.1016/j.mser.2005.07.001.
- [9] Hossein Taheri, "Friction Stir Welding." Accessed: Mar. 15, 2022. [Online]. Available: <https://encyclopedia.pub/18459>
- [10] Christian B. Fuller, "Friction Stir Tooling: Tool Materials and Designs," in *Friction Stir Welding and Processing*, Rajiv S. Mishra and Murray W. Mahoney, Eds. 2007, pp. 7–35.
- [11] S. Ahmed, A. Shubhrant, A. Deep, and P. Saha, "Development and Analysis of Butt and Lap welds in Micro Friction Stir Welding ( $\mu$ FSW)," 2014.
- [12] J. P. Martin, C. Stanhope, and S. Gascoyne, "NOVEL TECHNIQUES FOR CORNER JOINTS USING FRICTION STIR WELDING," *TMS 2011 Annual Meeting & Exhibition*, 2011, Accessed: Jan. 03, 2022. [Online]. Available: <https://www.twi-global.com/technical-knowledge/published-papers/novel-techniques-for-corner-joints-using-friction-stir-welding>
- [13] X. He, F. Gu, and A. Ball, "A review of numerical analysis of friction stir welding," *Progress in Materials Science*, vol. 65, Aug. 2014, doi: 10.1016/j.pmatsci.2014.03.003.
- [14] G. Padmanaban and V. Balasubramanian, "Selection of FSW tool pin profile, shoulder diameter and material for joining AZ31B magnesium alloy – An experimental approach," *Materials & Design*, vol. 30, no. 7, pp. 2647–2656, Aug. 2009, doi: 10.1016/j.matdes.2008.10.021.

- [15] A. Mishra, A. Tiwari, M. K. Shukla, and A. R. Rose, "Analysis of Tools used in Friction Stir Welding process," *International Journal of Current Engineering and Technology*, vol. 8, no. 6, Nov. 2018, doi: 10.14741/ijcet/v.8.6.2.
- [16] Wikipedia, "Rutilo." <https://it.wikipedia.org/wiki/Rutilo> (accessed Mar. 15, 2022).
- [17] Wikipedia, "Ilmenite." <https://it.wikipedia.org/wiki/Ilmenite> (accessed Mar. 15, 2022).
- [18] Gerd Lütjering and James C. Williams, *Titanium*, 2nd ed. Berlin, Heidelberg: Springer Berlin Heidelberg, 2007. doi: 10.1007/978-3-540-73036-1.
- [19] R. R. Boyer, "An overview on the use of titanium in the aerospace industry," *Materials Science and Engineering A*, vol. 213, no. 1–2, pp. 103–114, 1996, doi: 10.1016/0921-5093(96)10233-1.
- [20] V. Dhinakaran, S. V. Shriragav, A. F. Y. Fahmidha, and M. Ravichandran, "A review on the categorization of the welding process of pure titanium and its characterization," in *Materials Today: Proceedings*, 2020, vol. 27, pp. 742–747. doi: 10.1016/j.matpr.2019.12.034.
- [21] A. Fall, M. H. Fesharaki, A. R. Khodabandeh, and M. Jahazi, "Tool wear characteristics and effect on microstructure in Ti-6Al-4V friction stir welded joints," *Metals (Basel)*, vol. 6, no. 11, Nov. 2016, doi: 10.3390/met6110275.
- [22] S. Ji and Z. Li, "Reducing the Hook Defect of Friction Stir Lap Welded Ti-6Al-4V Alloy by Slightly Penetrating into the Lower Sheet," *Journal of Materials Engineering and Performance*, vol. 26, no. 2, pp. 921–930, Feb. 2017, doi: 10.1007/s11665-017-2512-2.
- [23] J. Su, J. Wang, R. S. Mishra, R. Xu, and J. A. Baumann, "Microstructure and mechanical properties of a friction stir processed Ti–6Al–4V alloy," *Materials Science and Engineering: A*, vol. 573, pp. 67–74, Jun. 2013, doi: 10.1016/j.msea.2013.02.025.
- [24] S. Mironov, Y. S. Sato, and H. Kokawa, "Development of grain structure during friction stir welding of pure titanium," *Acta Materialia*, vol. 57, no. 15, pp. 4519–4528, Sep. 2009, doi: 10.1016/j.actamat.2009.06.020.
- [25] H. Liu, K. Nakata, N. Yamamoto, and J. Liao, "Grain orientation and texture evolution in pure titanium lap joint produced by friction stir welding," *Materials Transactions*, vol. 51, no. 11, pp. 2063–2068, 2010, doi: 10.2320/matertrans.M2010242.
- [26] F. C. Liu, H. Liu, K. Nakata, N. Yamamoto, and J. Liao, "Investigation on friction stir welding parameter design for lap joining of pure titanium," *Proceedings of the 1st International Joint Symposium on Joining and Welding*, pp. 159–163, Jan. 2013, doi: 10.1533/978-1-78242-164-1.159.
- [27] H. Fujii, Y. Sun, H. Kato, and K. Nakata, "Investigation of welding parameter dependent microstructure and mechanical properties in friction stir welded pure Ti joints," *Materials Science and Engineering: A*, vol. 527, no. 15, pp. 3386–3391, Jun. 2010, doi: 10.1016/J.MSEA.2010.02.023.
- [28] W. B. Lee, C. Y. Lee, W. S. Chang, Y. M. Yeon, and S. B. Jung, "Microstructural investigation of friction stir welded pure titanium," *Materials Letters*, vol. 59, no. 26, pp. 3315–3318, Nov. 2005, doi: 10.1016/J.MATLET.2005.05.064.
- [29] I. K. Chernykh, E. v. Vasil'Ev, I. K. Chekalin, E. v. Krivonos, and D. S. Makashin, "Friction stir welding of titanium alloys OT-4 and VT-20," in *Journal of Physics: Conference Series*, May 2019, vol. 1210, no. 1. doi: 10.1088/1742-6596/1210/1/012030.

- [30] J. Wang, J. Su, R. S. Mishra, R. Xu, and J. A. Baumann, "Tool wear mechanisms in friction stir welding of Ti-6Al-4V alloy," *Wear*, vol. 321, pp. 25–32, 2014, doi: 10.1016/j.wear.2014.09.010.
- [31] G. Buffa, L. Fratini, F. Micari, and L. Settineri, "On the choice of tool material in friction stir welding of titanium alloys," in *Transactions of the North American Manufacturing Research Institution of SME*, 2012, vol. 40, pp. 785–794.
- [32] K. Reshad Seighalani, M. K. Besharati Givi, A. M. Nasiri, and P. Bahemmat, "Investigations on the Effects of the Tool Material, Geometry, and Tilt Angle on Friction Stir Welding of Pure Titanium," *Journal of Materials Engineering and Performance*, vol. 19, no. 7, pp. 955–962, Oct. 2010, doi: 10.1007/s11665-009-9582-8.
- [33] ESA, TWI, and Airbus D&S, "FRICTION STIR WELDED LOW-COST TITANIUM PROPELLANT TANK, PT. 1," Jun. 30, 2017. <https://www.twi-global.com/who-we-are/who-we-work-with/industry-sectors/aerospace/space/space-projects/friction-stir-welded-low-cost-titanium-propellant-tank-pt-1> (accessed Mar. 12, 2022).
- [34] ESA, TWI, and Airbus D&S, "FRICTION STIR WELDED LOW-COST TITANIUM PROPELLANT TANK, PT. 2," Jun. 30, 2017. <https://www.twi-global.com/who-we-are/who-we-work-with/industry-sectors/aerospace/space/space-projects/friction-stir-welded-low-cost-titanium-propellant-tank-pt-2> (accessed Mar. 12, 2022).
- [35] ESA, TWI, and Airbus D&S, "Friction stir welding for low-cost titanium propellant tanks," Jun. 30, 2017. <https://www.ukspacefacilities.stfc.ac.uk/Pages/TWI-Friction-stir-welding-for-low-cost-titanium-propellant-tanks.aspx> (accessed Mar. 12, 2022).
- [36] A. K. Singh *et al.*, "Friction stir welding of additively manufactured Ti-6Al-4V: Microstructure and mechanical properties," *Journal of Materials Processing Technology*, vol. 277, p. 116433, Mar. 2020, doi: 10.1016/J.JMATPROTEC.2019.116433.